博士論文

論文題目
MOLECULAR DYNAMICS SIMULATION OF
CHEMICAL REACTION USING TIME-DEPENDENT
FIRST-PRINCIPLES METHODS
（時間に依存する第一原理手法を用いた化学
反応の分子動力学シミュレーション）

横浜国立大学大学院
工学府

PHAM THI NU
13SD292

2017 年 3月

Table of Contents

List of Figures

List of Tables

Chapter 1

Introduction

In materials science, it is very important to simulate chemical reactions without actually performing experiments. With the advanced computing facilities, one can "see" how a chemical reaction progresses. Simulation helps us not only to confirm the experimental evidence but also to guide the experimental method. Theoretical physical-chemistry methods have had great success in predicting experimental results using different models and approximations. It is much easier to look for a successful synthesis route using theoretical calculations than through blind experimental trials, which are generally expensive and time-consuming. To study a chemical reaction, it is useful to analyze not only the structure of molecules, i.e., the position of atoms, but also the time evolution of the electronic state of the whole systems. One of the very well-known methods is molecular dynamics (MD).

MD is a technique for computing the equilibrium and nonequilibrium behaviours of a many-body system [1] by simulating the movements of atoms and molecules. It helps to understand the properties of the structure of the molecules as well as the interaction among atoms and molecules inside the system at the atomic level. By performing the MD simulation, one is able to (a) learn something new, something that cannot be observed directly by experiment, and (b) help to find the best way to perform the experiment. MD has been successfully employed to simulate biological processes such as protein folding, polymers, liquids, liquid solutions, and various materials involving structural and mechanical properties. Moreover, MD has been used for studying chemical reactions, enzyme catalysis, photochemical reaction, electron transfer etc. MD can be categorized into classical MD and *ab initio* or first-principle MD (AIMD). Classical MD using predefined potentials, i.e., force fields, that are provided by empirical data or independent electronic structure calculations [2]. Classical MD is faster than AIMD and simulations for very large systems as well as for long-time processes such as diffusion can be easily performed. However, many important systems have different atom or molecule types or the electronic structure and thus the chemical

bonding nature changes qualitatively during the course of the simulation. Therefore, in these systems, devising a fixed predefined potential becomes difficult and has serious drawbacks [3, 4]. In this regards, AIMD is required.

In an ab initio approach, strictly speaking, the full time-dependent Schrödinger equation has to be solved to get the complete description of a many-electron and nuclei system. However, this is an impossible task for the systems consisting of more than three nuclei and more than two electrons [5, 6]. Therefore, some important approximations have to be applied. The first very important approximation is the *Born-Oppenheimer* approximation [7, 8]. Because the mass of the electron is very small compared with the mass of the nucleus, one can consider that nuclei are moving very slowly relative to the electrons. It means that for the fixed nuclear configuration, a steady electronic quantum state can be obtained by solving the time-independent Schrödinger equation. And in this approximation, nucleus moves on a single potential energy surface (PES). In addition, to using the Born-Oppenheimer approximation, nuclei are considered as classical particles which obey the Newtonian equations of motion. Another important approximation is involved in a predefined set of one-electron functions, the so-called basis set, to express the molecular orbitals. AIMD has been applied successfully to study many complex systems with a high accuracy [2].

Recently, with the development of the femtosecond laser technology, and significant progress in theory of the electronic excited states, the fast chemical reactions at the femtosecond time-scale induced by excitations of electrons have gained a lot of interest experimentally [9] as well as theoretically [10]. For ground state systems of atoms and molecules, the AIMD simulations within the framework of density functional theory (DFT) have been applied successfully to study properties of the system. Runge-Gross theorem [11] has extended the application of DFT to the time-dependent systems. The time-dependent DFT (TDDFT) can be used to study the fast dynamics of the chemical reactions. In the TDDFT approach, the density functional of the exchange-correlation potential also needs to be approximated. For the ground state simulations, the adiabatic local density approximation (A-LDA) can be used for simplicity. On the other hand, for the excited state simulations, we do not know the explicit form of the exchange-correlation potential. Although, it is possible to use the A-LDA, but it is not so reliable. Instead, we propose to use the one-shot GW approximation (GWA) [12, 13, 14, 15] that treats the first-order contribution from

the self-energy (for the one-particle Green's function G) to first order with respect to the dynamically screened Coulomb interaction W given in the random-phase approximation (RPA). We call this method the time-dependent GW (TDGW) method. This is a simple extension of the so-called extended Hartree-Fock approximation for excited states [16]. Then we can perform the usual Ehrenfest dynamics simulation for the electronic excited state.

There are still some issues to be considered. In the case of a hydrogen atom, the quantum behavior of nuclei may be important. If we ignore this effect, it becomes necessary to comment on the validity of the treatment. For charge-transfer reactions or photochemistry processes, which happens around the crossing points of different electronic states, the adiabatic approximation becomes invalid. Out of many semiclassical approaches to non-adiabatic dynamics that have been proposed, the non-adiabatic quantum molecular dynamics (NAQMD), which was introduced by U. Saalmann [17], has some advantages. This method treats simultaneously the classical nuclear motion and quantum electronic excitations in dynamical processes of atomic many-body systems. Based on TDDFT, coupled non-linear equations of motion are derived for arbitrary basis sets for the time-dependent Kohn-Sham orbitals. Furthermore, it has the ability to make the approach practical for large atomic cluster systems.

The all-electron mixed basis approach (program name TOMBO [18]), which has been developed in our group [19, 20, 21], has many advantages in simulating and calculating electronic properties of materials. It has been applied successfully in many systems such as simulation of foreign atom insertion to C_{60} [22], light-harvesting π-conjugated dendrimer, thin film organic solar cell [23], attaching phenylene-vinylene to phthalocyanine, etc. TOMBO enables us to describe correctly the free-electron continuum states as well as the localized states in an all-electron formalism, because both plane waves and atomic orbital are used as basis functions. In the newest version of TOMBO, I have introduced the one-shot GW approximation for excited states MD simulation and implemented the NAQMD for a non-adiabatic process, which can perform both ground state and excited state MD with high accuracy.

The purpose of this thesis is to investigate the application of the first principles MD for the study of chemical reactions at atomic levels. With the new implementation of TDGW and NAQMD in the TOMBO program, I have performed successfully the simulation of the hydrogenation reaction of carbon monoxide. In this research, I have found one of the possible reaction pathways to create methanol from

carbon monoxide. In addition, a first principles all-electron study of the oxirane molecule at excited states was performed. The results contribute a possible discussion on the involving excited states of photochemical ring opening of this molecule.

This thesis is composed of five chapters. In the second chapter, I will give a brief description of the general theory of AIMD and the all-electron mixed basis approach. The next section, Chapter 3, will present the AIMD simulation study of successive hydrogenation reactions of carbon monoxide producing methanol. This chapter interpolates material form the paper which was published by author [24]. Chapter 4 contains the *ab initio* all electron study of photochemical ring opening of oxirane molecule. I present the conclusions and briefly discuss the extension of the present work in Chapter 5.

Chapter 2

General Theory

Molecular dynamics simulations process are similar with performing a real experiment in someway. In experiment, we prepare a sample, connect to a measuring instrument, and then measure the interested property [1]. In MD simulation, we choose a model, set the necessary input: the atoms positions, velocities, and masses, and calculate the material properties. The simulation is split into variety of time steps, in every time step all the forces between all the atoms are calculated so integrated to get new positions and velocities. This is often iterated to the top of the simulation. Throughout the time steps material properties is calculated from the positions, velocities and forces.

Ab Initio Molecular Dynamics (AIMD) [28] typically refers to a mixed quantum and classical kind of MD. In this approach, the potential energy surface is obtained by a quantum mechanical electronic structure method while nuclei are considered as classical particles. In this chapter, I am going to explain the theoretical background of AIMD and introduce about the non-adiabatic quantum molecular dynamics (NAQMD) as well as the time-dependent GW method (TDGW).

2.1   Theoretical background

A fully description of a many body system can be derived from the time dependent Schrödinger equation [27]

$$H\Psi(\{\mathbf{r}_i\}, \{\mathbf{R}_I\}, t) = i\hbar \frac{\partial}{\partial t} \Psi(\{\mathbf{r}_i\}, \{\mathbf{R}_I\}, t), \tag{2.1}$$

here $\{\mathbf{R}_I\} = (\mathbf{R}_1, \mathbf{R}_2, , \mathbf{R}_I, , \mathbf{R}_N)$ are the nuclei coordinates, and electrons located at $\{\mathbf{r}_i\} = (\mathbf{r}_1, \mathbf{r}_2, , \mathbf{r}_I, , \mathbf{r}_N)$. H is total Hamiltonian which can be written as

$$H(\{\mathbf{r}_i\}, \{\mathbf{R}_I\}) = T_n(\{\mathbf{R}_I\}) + T_e(\{\mathbf{r}_i\}) + V_{n-n}(\{\mathbf{R}_I\}) + V_{n-e}(\{\mathbf{r}_i\}, \{\mathbf{R}_I\}) + V_{e-e}(\{\mathbf{r}_i\}), \qquad (2.2)$$

where $T_n(\{\mathbf{R}_I\})$ is kinetic energy of the atomic nuclei

$$T_n(\{\mathbf{R}_I\}) = -\sum_I \frac{\hbar^2}{2M_I} \nabla_I^2,$$

$T_e(\{\mathbf{r}_I\})$ is kinetic energy of the electrons

$$T_e(\{\mathbf{r}_i\}) = -\sum_i \frac{\hbar^2}{2m_e} \nabla_i^2,$$

internuclear repulsion $V_{n-n}(\{\mathbf{R}_I\})$

$$V_{n-n}(\{\mathbf{R}_I\}) = \frac{1}{4\pi\epsilon_0} \sum_{I<J} \frac{e^2 Z_I Z_J}{|\mathbf{R}_I - \mathbf{R}_J|},$$

electronic nuclear attraction $V_{n-e}(\{\mathbf{r}_i\}, \{\mathbf{R}_I\})$

$$V_{n-e}(\{\mathbf{r}_i\}, \{\mathbf{R}_I\}) = -\frac{1}{4\pi\epsilon_0} \sum_{I,i} \frac{e^2 Z_I}{|\mathbf{R}_I - \mathbf{r}_j|},$$

and interelectronic repulsion $V_{e-e}(\{\mathbf{r}_i\})$

$$V_{e-e}(\{\mathbf{r}_i\}) = \frac{1}{4\pi\epsilon_0} \sum_{i<j} \frac{e^2}{|\mathbf{r}_i - \mathbf{r}_j|}.$$

Here m_e is the electron mass, M_I and Z_I are the mass and atomic number of the *Ith* nuclear. The total Hamiltonian can be rewritten as:

$$H(\{\mathbf{r}_i\}, \{\mathbf{R}_I\}) = T_n(\{\mathbf{R}_I\}) + H_{el}(\{\mathbf{r}_i\}, \{\mathbf{R}_I\}), \qquad (2.3)$$

where $H_{el}(\{\mathbf{r}_i\}, \{\mathbf{R}_I\})$ is the Hamiltonian of electronic parts. For a *fixed* nuclear configuration, we have the time-independent (electronic) Schrödinger equation:

$$H_{el}(\{\mathbf{r}_i\}, \{\mathbf{R}_I\})\Phi_k(\{\mathbf{r}_i\}, \{\mathbf{R}_I\}) = E_k(\{\mathbf{R}\})\Phi_k(\{\mathbf{r}_i\}, \{\mathbf{R}_I\}). \tag{2.4}$$

Here the $\Phi_k(\{\mathbf{r}_i\}, \{\mathbf{R}_I\})$ are considered as the adiabatic state or Born-Oppenheimer state. The spectrum of $H_{el}(\{\mathbf{r}_i\}, \{\mathbf{R}_I\})$ is assumed to be discrete and the eigenfunctions are orthonormalized

$$\int_{-\infty}^{\infty} \Phi_k^*(\{\mathbf{r}_i\}, \{\mathbf{R}_I\})\Phi_l(\{\mathbf{r_i}\}, \{\mathbf{R}_I\})d\mathbf{r} \equiv \langle \Phi_k | \Phi_l \rangle = \delta_{kl}. \tag{2.5}$$

The total wavefunction Ψ can be expanded in terms of the eigenfunctions of H_{el} because they form a complete set

$$\Psi(\{\mathbf{r}_i\}, \{\mathbf{R}_I\}, t) = \sum_k \Phi_k(\{\mathbf{r}_i\}, \{\mathbf{R}_I\})\chi_k(\{\mathbf{R}_I\}, t), \tag{2.6}$$

where $\chi_k(\{\mathbf{R}_I\}, t)$ are the nuclear wavefunction, which does not depend on $\mathbf{r}_i$, so can be consider as expansion coefficient at the time t. This is an ansatz introduced by Born in 1951 [7, 8]. Insertion this ansatz into the time-dependent Schrödinger equation Eq. (2.1), multiplying from the left by $\Phi_k^*(\{\mathbf{r}_i\}, \{\mathbf{R}_I\})$ and the integration with respect to over the electronic coordinates results in a set of coupled differential equations

$$\left[-\sum_I \frac{\hbar^2}{2M_I}\nabla_I^2 + E_k(\{\mathbf{R}_I\}) \right]\chi_k + \sum_I C_{kl}\chi_l = i\hbar\frac{\partial}{\partial t}\chi_k \tag{2.7}$$

with

$$C_{kl} = \int \Psi_k^* \left[-\sum_I \frac{\hbar^2}{2M_I}\nabla_I^2 \right]\Psi_l d\mathbf{r} + \frac{1}{M_I}\Sigma_I \left\{ \int \Psi_k^*[-i\hbar\nabla_I]\Psi_l d\mathbf{r} \right\}[-i\hbar\nabla_I]. \tag{2.8}$$

The matrix elements C_{kl} mean the coupling between different states.

2.1.1 Adiabatic molecular dynamics

In the Born-Oppenheimer approximation [8] where all of the coupling matrix elements are neglected, the equation (2.7) becomes

$$\Big[- \sum_I \frac{\hbar^2}{2M_I} \nabla_I^2 + E_k(\{\mathbf{R_I}\}) \Big] \chi_k = i\hbar \frac{\partial}{\partial t} \chi_k. \tag{2.9}$$

In the adiabatic molecular dynamics, based on the Born-Oppenheimer approximation, the transitions between different potential energy surfaces are neglected, the equation of nuclei are described simply by the Newton's equation:

$$M_I \ddot{\mathbf{R}}_I = -\frac{\partial E_k}{\partial \mathbf{R}_I}. \tag{2.10}$$

The adiabatic molecular dynamics are valid in the large energy band gaps systems and nuclei have small velocities (characterised by the Massay parameter [25]). However, when the level crossing occur, the so-called nonadiabatic treatment is required.

2.1.2 Mixed quantum - classical non-adiabatic molecular dynamics

In principle, in the adiabatic molecular dynamics, the electronic transitions are neglected and the system evolves in only one electronic state. In the systems, which have the crossing between energy levels, the electronic transitions among different states can not be ignored, so that the non-adiabatic treatment is required. Two main approaches of non-adiabatic molecular dynamics are Ehrenfest approach and trajectory surface hopping approach [28].

Ehrenfest molecular dynamics

In Ehrenfest molecular dynamics, the total wavefunction is written as

$$\Psi(\mathbf{r}, \mathbf{R}, t) = \chi(\mathbf{R}, t)\phi(\mathbf{r}, t) \exp\Big[i \int^t dt' E_e(t')\Big]. \tag{2.11}$$

In this approach, the electronic state is time-dependent instead of the time-independent state in the adiabatic approximation. Inserting this wave function to the time-dependent Schrödinger equation Eq. (2.1),

taking the classical limit will get two equations of motion for electronic motion

$$i\frac{\partial}{\partial t}\phi(\mathbf{r}, t) = H_{el}(\mathbf{r}, \mathbf{R})\phi(\mathbf{r}, t), \tag{2.12}$$

and for nuclei

$$M_I\ddot{\mathbf{R}}_I = -\frac{\partial}{\partial \mathbf{R}_I} \langle \phi_I(t)| H_{el}(\mathbf{R}) |\phi_I(t)\rangle. \tag{2.13}$$

Nuclei move on the effective potential energy surface of the average over the electronic subsystem. Applying the Hellman-Feynman theorem, the force acting to nuclei can be written as:

$$F = -\langle \phi| \nabla_{\mathbf{R}} H_{el} |\phi\rangle. \tag{2.14}$$

It is known that in the Ehrenfest approach, the electron-nuclear correlations are missing because the nuclear dynamics proceeds classically on a time-dependent effective potential [25]. It can not applied in the cases potential energy surfaces exhibit a very different behaviour.

Trajectory surface hopping approach

This approach extends excited state molecular dynamics in a stochastic scheme to treat non-adiabatic transitions. The equation of motions of electron and nuclei are written in the next two equations:

$$i\frac{\partial}{\partial t}c_I(t) = E_I(\mathbf{R})c_I(t) - i\sum_J\sum_I \dot{\mathbf{R}}_I \cdot \mathbf{D}^I_{IJ}c_J(t) \tag{2.15}$$

$$M_I\ddot{\mathbf{R}}_I = -\frac{\partial E_I}{\partial \mathbf{R}_I}. \tag{2.16}$$

Here $c_I(t)$ are the expansion coefficients $\phi(\mathbf{r}, t) = \sum_I c_I(t)\phi(\mathbf{r}, \mathbf{R})$ and $\mathbf{D}^I_{IJ} = \left\langle \phi_I(\mathbf{R})\left|\frac{\partial}{\partial R}\phi_J(\mathbf{R})\right.\right\rangle$ are the nonadiabatic coupling term. The surface switching scheme is defined by the transition probability, that can be calculated from $c_I(t)$. The widely used trajectory surface hopping methods is Tullys fewest switches algorithm [26]. In the fewest switches surface hoping method, the number of hops between different electronic states is minimized. The non-adiabatic transitions describe the quantum effect of nuclear motion to electronic motion. However, this method can only apply for a small system with limited number of quantum degrees of freedom and still based on the separation of classical (nuclei) and quantum (electronic)

part.

2.2 Electronic structure method

There is no empirical potential in AIMD, thus the time-independent Schrödinger equation, Eq.(2.4), should in principle to be solved directly. However, it is an impossible task except for hydrogen atom. There are wave function based approaches and density functional theory approach (DFT). Some very famous wave function based approaches are Hartree-Fock (HF), Multi-Configurational Self-Consistent Field (MCSCF), and the Coupled Cluster (CC) method. In many systems, DFT method gives the good result while take less computational cost than the wave function based method. In this section, the (time-dependent) density functional theory is going to presented.

2.2.1 Density functional theory

DFT is well written in many textbooks, such as [29, 30]. In DFT the central quantity is the electronic (spin) density $n(\mathbf{r})$, that depends only on 3 spatial coordinates plus a spin coordinate in the case of spin polarized DFT. This provides a considerable simplification compared to wavefunction based methods, in which the N-electron wavefunction depends on 3N spatial plus N spin coordinates [31]. The two Hohenberg-Kohn (HK) theorems [32], provide a way to determine the properties of a system only on the basis of its electron density. The first theorem states that the external potential V_{ext} of a system is (up to a constant) uniquely determined by the ground-state density n_0. Since hamiltonian depends on V_{ext}, it depends also on the density and therefore the true electronic ground state and all its properties are determined by n_0. Thus the ground-state energy E_0 can be written as a functional of n_0

$$E_0[n_0] = E_{N_e}[n_0] + T[n_0] + E_{ee}[n_0], \tag{2.17}$$

where E_{N_e} is a system dependent part, defined by the positions $\mathbf{R}_I$ and charges Z_I of the nuclei through the external potential V_{ext}, $T[n]$ is the kinetic energy of the electrons and E_{ee} is the electron-electron interaction. $T[n]$ and E_{ee} define the system independent part. The system independent functional is called

the universal or HK functional

$$F[n] = T[n] + E_{ee}[n]. \tag{2.18}$$

The second HK theorem provides a way to determine the true ground-state density n_0 of a system. Based on the variational principle, it states that the trial density $\tilde{n}$, that minimizes the ground-state energy functional E_0, is equal to the true ground-state density n_0 of the system. Therefore, any density $\tilde{n}$, that satisfies certain boundary conditions, provides an upper bound of the true ground-state energy

$$E[\tilde{n}] = \int V_{ext}(\mathbf{r})\tilde{n}(\mathbf{r})d\mathbf{r} + F[\tilde{n}] \geq E_0 = E[n_0]. \tag{2.19}$$

Provided that we know the expression for the universal functional we are in principle able to search for the ground-state energy, by minimizing $E[\tilde{n}]$ in some way. Still, we do not know the exact dependence of the electronic kinetic energy on the density and so the exact relationship between the non-classical electron-electron interaction and the density is unknown.

2.2.2 Time-independent Kohn-Sham equations

The local-density approximation (LDA) or Kohn-Sham ansatz was introduced by Kohn and Sham [33]. They proposed that there is a non-interacting system that has the same ground state density with the interacting system. Within this approximation, the electrons will interact through an effective potential. Thus, instead of solving the system of interacting particles in the presence of the external potential, one can solve the system of non-interacting particles in an effective potential. In the Kohn-Sham approach, $T[n]$ and $E_{ee}[n]$ are split each into two parts

$$T[n] = T_S[\{\psi_i\}] + T_C[n] \tag{2.20}$$

$$E_{ee}[n] = J[n] + E_{ncl}[n]. \tag{2.21}$$

$T_S[\{\psi_i\}]$ denotes the electronic kinetic energy of a non-interacting reference system and $E_{ncl}[n]$ stands for the non-classical electron-electron interaction terms. The electrons of the non-interacting system are

described by orbitals ψ_i, satisfying

$$\sum_i^N |\psi_i(\mathbf{r})|^2 = n(\mathbf{r}), \tag{2.22}$$

where it is assumed that the density of the reference system n is equal to the true density n_0 of the system ($n = n_0$). T_C is defined as the difference between the kinetic energy of the interacting system and T_S and arises due to the interaction of the electrons including all quantum effects. The advantage of this splitting is that by introducing non-interacting orbitals ϕ_i that integrate to n, T_S can be determined in the same way as in Hatree - Fock theory

$$T_S[\psi_i] = -\frac{1}{2} \sum_i \langle \psi_i | \nabla^2 | \psi_i \rangle. \tag{2.23}$$

The term $J[n]$ in the second equation is just the classical Coulomb energy

$$J[n] = \frac{1}{2} \int \int \frac{n(\mathbf{r})n(\mathbf{r'})}{|\mathbf{r} - \mathbf{r'}|} \mathbf{r}d\mathbf{r'} \tag{2.24}$$

and E_{ncl} is the non-classical contribution of the electron-electron interaction energy. Here we use the atomic units, where we put $e = m = \hbar = 1$. The remaining quantities $E_{ncl}[n]$ and $T_C[n]$ are still unknown. However, the KS approach relies on the assumption that these two quantities are rather small compared to the other terms and that they can be approximated in some way. By defining the exchange correlation functional $E_{xc}[n]$

$$E_{xc}[n] = T_C[n] + E_{ncl}[n], \tag{2.25}$$

the HK functional can be rewritten as

$$F[n] = T_S[\{\psi_i\}] + J[n] + E_{xc}[n]. \tag{2.26}$$

Thus we have an approximation for E_{xc}, the ground-state energy E_0 can be found by minimizing the functional

$$E_0[n] = E_{N_e}[n] + T_S[\psi_i] + J[n] + E_{xc}[n] \tag{2.27}$$
$$= -\sum_i \int \sum_I \frac{Z_I}{|\mathbf{R_I} - \mathbf{r}|}|\psi_i(\mathbf{r})|^2 d\mathbf{r}$$

$$-\frac{1}{2}\sum_i \langle \psi_i | \nabla^2 | \psi_i \rangle$$

$$+\frac{1}{2}\sum_{ij} \int \int |\psi_i(\mathbf{r})|^2 \frac{1}{|\mathbf{r}-\mathbf{r}'|}|\psi_j(\mathbf{r}')|^2 d\mathbf{r}d\mathbf{r}' + E_{xc}[n].$$

Similarly to HF theory, minimization of E_0 can be carried out by solving self-consistently a set of equations, for non-interacting electrons moving in an effective potential, called as Kohn-Sham potential V^{KS},

$$[-\frac{1}{2}\nabla^2 + V^{KS}(\mathbf{r})]\psi_i(\mathbf{r}) = \epsilon_i\psi_i(\mathbf{r}) \tag{2.28}$$

that yields the optimal non-interating orbitals. The difference with HF theory lies in the form of the effective potential

$$V^{KS}(\mathbf{r}) = V_{xc}(\mathbf{r}) + \int \frac{n(\mathbf{r}')}{|\mathbf{r}'-\mathbf{r}|}d\mathbf{r}' - \sum_I \frac{Z_I}{|\mathbf{R}_I - \mathbf{r}|} \tag{2.29}$$

with

$$V_{xc} = \frac{\delta E_{xc}[n]}{\delta n}. \tag{2.30}$$

The optimized orbitals ψ_i of Eq. (2.28), are called *Kohn-Sham* orbitals and differ from the HF orbitals.

The remaining task consists in finding a good approxiamtion for the exchange-correlation term. One of the major approaches is the local density approximation (LDA), as it is local in sense that $E_{xc}^{LDA}[n(\mathbf{r})]$ depends only $n(\mathbf{r})$.

$$E_{xc}^{LDA}[n(\mathbf{r})] = \int n(\mathbf{r})\epsilon_{xc}[n(\mathbf{r})]d\mathbf{r}, \tag{2.31}$$

where ϵ_{xc} is the exchange-correlation energy per particle of a homogeneous electron gas of charge density $n(\mathbf{r})$.

2.2.3 Time-dependent density functional theory

The application of DFT was limited within the ground state. For excited state, the time-dependent extension of DFT method, the so-called time-dependent density functional theory (TDDFT) is applied widely. TDDFT was established based on the Rung-Gross theorem [11]. This theorem states that there is a one-to-one mapping between the time-dependent one-body density $n(\mathbf{r}, t)$ and the time-dependent external

potential $V_{ext}(\mathbf{r}, t)$. At the time $t = 0$, we have $\phi(t_0) = \phi_O$ and at the time t, $\phi(t) = \phi[n, \phi(t_0)] \exp[-i\alpha(t)]$. Here α is a phase factor. A detailed proof of the Runge-Gross theorem is presented in [30].

The Kohn-Sham system, a imaginary system with non-interacting particles, again helps the Rung-Gross theorem becomes applicable. The time-dependent Kohn-Sham equations can be written as follows:

$$i\frac{\partial}{\partial t}\psi_i(\mathbf{r}, t) = \left[-\frac{\nabla^2}{2} + V^{KS}(\mathbf{r}, t) \right]\psi_i(\mathbf{r}, t).$$

(2.32)

Here $\psi_i(\mathbf{r}, t)$ is the Kohn-Sham wave function of non-interacting particle, $V^{KS}(\mathbf{r}, t)$ is the Kohn-Sham potential, being the sum of the external potential V_{ext}, the Hartree potential and the exchange potential V_{xc}

$$V^{KS}(\mathbf{r}, t) = V_{ext}(\mathbf{r}, t) + \int d^3\mathbf{r}' \frac{n(\mathbf{r}', t)}{|\mathbf{r} - \mathbf{r}'|} + V_{xc}(\mathbf{r}, t).$$

(2.33)

The explicit form of the exchange correlation is unknown. Van Leeuwen has defined an action functional $\tilde{A}$ [34] based on Keldish formalism. The time-dependent exchange correlation potential is approximated as

$$V_{xc}(\mathbf{r}, t) \approx \frac{\delta E_{xc}}{\delta n(\mathbf{r})}.$$

(2.34)

This approximation was called as the adiabatic local density approximation (A-LDA), in which the V_{xc} depends only on the density at that particular time, not on the time evolution of the density.

2.3 Non-adiabatic quantum molecular dynamics

The non-adiabatic quantum molecular dynamics (NAQMD) was introduced by U. Saalman [17] in 1996. As other normal mixed-quantum classical approach, NAQMD coupled the quantum mechanical treatment of the electrons within TDDFT in basis expansion with classical dynamics for the ions. This method can be able to study the dynamics of many systems include atoms, molecules.

At first, the classical part (nuclei) and quantum part (electrons) are separated in the Born-Oppenheimer approximation. And then, equations of motion for nuclei and electrons are obtained from the Ehrenfest theory under the requirement that the total energy is conserved. The description of electron part is derived

by TDDFT method within the Kohn-Sham approximation

$$i\frac{\partial \psi_i(\mathbf{r}, t)}{\partial t} = \left[-\frac{1}{2}\nabla^2 + V^{KS}(\mathbf{r}, t) \right]\psi_i(\mathbf{r}, t), \tag{2.35}$$

where ψ_i are the wave packet of non-interacting Kohn-Sham particles, in the effective potential V^{KS},

$$V^{KS}(\mathbf{r}, t) = -\sum_I \frac{Z_I}{|\mathbf{r} - \mathbf{R}_I|} + \int d\mathbf{r}' \frac{n(\mathbf{r}')}{|\mathbf{r} - \mathbf{r}'|} + V_{xc}(\mathbf{r}, t). \tag{2.36}$$

Here V_{xc} is the exchange-correlation potential. The explicit form of $V_{xc}(\mathbf{r}, t)$ is unknown, therefore has to be approximated in calculation. We have applied the adiabatic local density approximation (A-LDA) in the new implementation of NAQMD. The Kohn-Sham functions are expanded into basis function $\phi_\alpha(\mathbf{r}, \mathbf{R})$ as

$$\psi_i(\mathbf{r}, t) = \sum_{\alpha i} a_{i\alpha}(t)\phi_\alpha(\mathbf{r}, \mathbf{R}_\alpha). \tag{2.37}$$

The time-dependent electronic density is written as follows:

$$\rho(\mathbf{r}, t) = \sum_{j=1} N_e \sum_{\alpha\beta} a_{i\alpha}^*(t)a_{i\beta}^*(t)\phi_\alpha^*(\mathbf{r}, \mathbf{R}_\alpha)\phi_\beta(\mathbf{r}, \mathbf{R}_\beta). \tag{2.38}$$

Thus the time-dependent Kohn Sham equations is rewritten as

$$i\dot{a}_{\alpha i}(t) = \sum_{\beta\gamma} (S_{\alpha\beta}^{-1})\Big\{H_{\beta\gamma} - i\sum_I \mathbf{R}_I d_{\beta\gamma}^I\Big\}a_{\gamma i}(t) \tag{2.39}$$

where $S_{\alpha\beta}$ is the overlap matrix

$$S_{\alpha\beta} = \langle \phi_\alpha | \phi_\beta \rangle, \tag{2.40}$$

$H_{\alpha\beta}$ is the Hamiltonian matrix

$$H_{\alpha\beta} = \langle \phi_\alpha | -\frac{1}{2}\nabla^2 + V^{KS} |\phi_\beta \rangle, \tag{2.41}$$

and $\mathbf{d}_{\alpha\beta}^I$ is the nonadiabatic coupling vector matrix

$$\mathbf{d}_{\alpha\beta}^I = \langle \phi_\alpha | \nabla_I |\phi_\beta \rangle. \tag{2.42}$$

The corresponding equations of motion for the classical nuclei in term of these above matrixes can be written as

$$M_I \ddot{\mathbf{R}}_I = -\nabla_I \sum_J \frac{Z_I Z_J}{|\mathbf{R}_I - \mathbf{R}_J|} - \sum_j \left\{ \sum_{\alpha\beta} a^*_{\alpha j} [\nabla_I H_{\alpha\beta} - \langle \phi_\alpha | \nabla_I (V_H + V_{xc}) |\phi_\beta \rangle] a_{\beta j} \right.$$

$$\left. - \sum_{\alpha\beta\gamma\sigma} a^*_{\alpha j} [H_{\alpha\beta} (S^{-1}_{\beta\gamma}) \mathbf{d}^I_{\gamma\sigma} + (\mathbf{d}^T)^I_{\alpha\beta} (S^{-1}_{\beta\gamma}) H_{\gamma\sigma}] a_{\sigma j} \right\}. \tag{2.43}$$

NAQMD method is defined by the electronic and nuclear equations of motion (2.39) and (2.43)[17]). These two equations have to be solved self-consistently to get the description of the system. Here it is important to note that the force acting on nuclei is given by an average over the quantum mechanical subsystem, so the NAQMD represents an Ehrenfest approach. And the electron-nuclei correlations are neglected in this approach.

By applying NAQMD to the collision of a hydrogen atom with a proton, U. Saalmann [17] has presented the effects of non-adiabatic transitions on the motion of the nuclei by using NAQMD to describe the collision of a proton with a hydrogen atom. NAQMD also has been applied to simulate other systems such as the collision of atom and cluster, the collision of ion to fullerene molecule [35, 36, 37, 38].

2.4 Molecular dynamics based on time-dependent density functional theory

Our method of *ab inito* molecular dynamics based on time-dependent density functional theory (TDDFT) [40, 41, 42, 22] can be described briefly as following. Atomic units are used in all formulation. For electronic part, the TDDFT was applied and the time-dependent Kohn-Sham (TDKS) equation is written as

$$i \frac{\partial}{\partial t} |\psi_i(\mathbf{r}, t)\rangle = H_{el} |\psi_i(\mathbf{r}, t)\rangle. \tag{2.44}$$

Nuclear motion is governed by the Newtonian equation

$$M_A \frac{d^2 \mathbf{R}_A}{dt^2} = -\frac{\partial}{\partial \mathbf{R}_A} \left[\langle E_{el} \rangle + \sum_B \frac{Z_A Z_B}{|\mathbf{R}_A - \mathbf{R}_B|} \right], \tag{2.45}$$

where $H_{el}(r, t)$ is the electronic part of the Hamiltonian. $\langle E_{el} \rangle$ presents the expectation value of the electronic part of the total energy leading to the mean field potential for nuclei. $\mathbf{r}$ is the position of the electrons, while Z_A, M_A and $\mathbf{R}_A$ denote the number of nuclei, mass and the position of nucleus A, respectively. We have implemented the NAQMD method [17] to our program by the updating of wave packet. In the present study, adiabatic local density approximation (A-LDA) is used to obtain the exchange-correlation energy in TDDFT approach for electronic part. The spectral method [45] is used to integrate Eq.(2.44), other methods could be found in [43, 44] . At the initial time step $t = 0$,

$$\psi_i(\mathbf{r}, t = 0) = \phi_i(\mathbf{r}, t = 0). \tag{2.46}$$

At each time step, the eigenvalue problem of the electronic Hamiltonian is solved

$$H_{el}(\mathbf{r}, t) |\phi_k(\mathbf{r}, t)\rangle = \epsilon_k(t) |\phi_k(\mathbf{r}, t)\rangle. \tag{2.47}$$

here $\phi_k(\mathbf{r}, t)$ is the eigenstate of $H_{el}(\mathbf{r}, t)$ corresponding with the eigenvalues $\epsilon_k(t)$. During the small step Δt, in which Hamiltonian is considered almost no change, the TDKS equation (2.28) can be integrated as follows. The wave packets $\psi_j(\mathbf{r}, t)$ can be expanded in terms of the eigenstates $\phi_k(\mathbf{r}, t)$ at the time t as

$$
\begin{aligned}
|\psi_i(\mathbf{r}, t + \Delta t)\rangle &= \exp\left[-\frac{i}{\hbar} \int_t^{t+\Delta t} H_{el}(t')dt'\right] |\psi_i(\mathbf{r}, t)\rangle \\
&= \sum_k \exp\left[\frac{i}{\hbar} \int_t^{t+\Delta t} H_{el}(t')dt'\right] |\phi_k(\mathbf{r}, t + \Delta t)\rangle \langle\phi_k(\mathbf{r}, t + \Delta t)|\psi_i(\mathbf{r}, t)\rangle \\
&\approx \sum_k \exp\left[-\frac{i}{\hbar}\epsilon_k(t + \Delta t)\Delta t\right] |\phi_k(\mathbf{r}, t + \Delta t)\rangle \left\{ \langle\phi_k(\mathbf{r}, t)|\psi_i(\mathbf{r}, t)\rangle + \Delta t \frac{\partial}{\partial t'} \langle\phi_k(\mathbf{r}, t')|\psi_i(\mathbf{r}, t)\rangle_{t'=t} \right\}.
\end{aligned}
\tag{2.48}
$$

Within the adiabatic approximation, as the first order of approximation, one can assume

$$\frac{\partial}{\partial t'} \langle\phi_k(\mathbf{r}, t')|\psi_i(\mathbf{r}, t)\rangle_{t'=t} = 0. \tag{2.49}$$

and then the Kohn-Sham equation can be integrated as follows:

$$|\psi_i(\mathbf{r}, t + \Delta t)\rangle = \sum_k \exp\left[-\frac{i}{\hbar}\epsilon_k(t)\Delta t\right] |\phi_k(\mathbf{r}, t)\rangle \langle\phi_k(\mathbf{r}, t)|\psi_i(\mathbf{r}, t)\rangle. \tag{2.50}$$

One can consider nonadiabatic approximation as the second order of approximation:

$$|\psi_i(\mathbf{r}, t + \Delta t)\rangle \approx \sum_k \exp\left[-\frac{i}{\hbar}\epsilon_k(t)\Delta t\right] |\phi_k(\mathbf{r}, t)\rangle \left\{\langle\phi_k(\mathbf{r}, t)|\psi_i(\mathbf{r}, t)\rangle + \Delta t\frac{\partial}{\partial t'}\langle\phi_k(\mathbf{r}, t')|\psi_i(\mathbf{r}, t)\rangle_{t'=t}\right\}. \tag{2.51}$$

Let's investigate more detail the term $\frac{\partial}{\partial t'}\langle\phi_k(\mathbf{r}, t')|\psi_i(\mathbf{r}, t)\rangle_{t'=t}$ in terms of basis representation. Using the basis functions $\{|\xi\rangle\}$, we expanded the wave-packet $|\psi_i(\mathbf{r}, t)\rangle$ and the eigenfunction $|\phi_k(\mathbf{r}, t)\rangle$:

$$|\psi_i(\mathbf{r}, t)\rangle = \sum_m c_{im} |\xi_m\rangle \tag{2.52}$$

$$|\phi_k(\mathbf{r}, t)\rangle = \sum_l c_{kl} |\xi_l\rangle \tag{2.53}$$

so we have:

$$\begin{aligned}
\frac{\partial}{\partial t'}\langle\phi_k(\mathbf{r}, t')|\psi_i(\mathbf{r}, t)\rangle_{t'=t} &= \sum_I \dot{\mathbf{R}}_I \cdot \sum_{lm} \bar{c}_{kl}^*(\nabla_j \langle\xi_l|\xi_m\rangle)c_{im} \\
&= -\sum_I \sum_{lm} \bar{c}_{kl}^* \dot{\mathbf{R}}_I \cdot \mathbf{d}_{lm} c_{im}.
\end{aligned} \tag{2.54}$$

Here $\mathbf{d_{lm}}$ is the nonadiabatic coupling vector

$$\mathbf{d_{lm}} = \langle\xi_l| \nabla |\xi_m\rangle \tag{2.55}$$

and $\dot{\mathbf{R}}$ is the velocity of nuclear. The term describes the nonadiabatic effect is the product of nonadiabatic coupling vector and velocity of nuclear. It helps to reinforce that when no electronic transition occurs and the velocity of nuclei is small, the adiabatic approximation is good enough to describe the system.

Because the eigenstates $\phi_k(\mathbf{r})$ is changing with time, the compatible between the coefficients c_{ik} and eigenfunctions $\phi_i(\mathbf{r}, t = 0)$ will be difficult to determined. In other words, it is impossible to express the

time evolution of the electron wave packet as a superposition of the initial eigenstate. For this reason, only in the case the electronic states change very little from the initial state, the time evolution of the electron wave packets can be approximated as a superposition of the initial specific state. To check the change of the eigenstate during time, we need to compare the TDKS eigenvalue ϵ_k and the expectation values of Kohn-Sham Hamiltonian $\langle \psi_k | H | \psi_k \rangle$. Through out the time of simulation, the eigenvalues and expectation values are not much different, the electronic state can be consider as not the result of mixing with other states [46].

2.5   All-electron mixed basis approach

In spectral method, complete basis sets are required to expand the Kohn-Sham wave function. Our group has developed the all-electron mixed basis approach, which is the extension of the mixed basis approach introduced by Louie et al.[39] within the pseudopotential formalism. Both Plane wave (PWs) and Atomic Orbital (AOs) are used to expand the Kohn-Sham wavefucntions

$$\psi_i(\mathbf{r}) = \frac{1}{\sqrt{\Omega}} \sum_{\mathbf{G}} c_i^{PW}(\mathbf{G}) e^{i\mathbf{G}.\mathbf{r}} + \sum_i \sum_{nlm} c_j^{AO}(jnlm) \phi_{jnlm}^{AO}(\mathbf{r} - \mathbf{R}_i) \equiv \sum_{\xi} c_{i,\xi} f_{\xi}(\mathbf{r}), \tag{2.56}$$

where $\phi_{jnlm}^{AO}(\mathbf{r})$ represent atomic orbital functions, $\mathbf{G}$ is the reciprocal vector, Ω denotes the volume of a unit cell, j, n, l, m are the atomic species, the principal, angular-momentum and magnetic quantum numbers, respectively. c_ν^{PW} and c_ν^{AO} are the expansion coefficients corresponding with PWs and AOs. However, the expansion coefficients is the coefficients corresponding with the basis functions, different from the expansion factor for the specific state in the spectral method. To determine the Kohn-Sham energy eigenvalues ϵ_k, the generalized eigenvalue equation has to be solved because the basis functions $f_{\xi}(\mathbf{r})$ are not orthogonal to each other

$$\sum_{\xi'} H_{\xi\xi'} c_{k,\xi'} = \epsilon_k \sum_{\xi'} S_{\xi\xi'} c_{k,\xi'}, \tag{2.57}$$

where $H_{\xi\xi'} = \left\langle f_\xi \middle| H \middle| \xi \right\rangle$ are the Hamiltonian and $S_{\xi\xi'} = \left\langle f_\xi \middle| f'_\xi \right\rangle$ denote overlap matrix elements sandwiched by the ξth and ξth basis functions. Using the column vector

$$\Phi_k \equiv \begin{pmatrix} c_{k,1} \\ c_{k,2} \\ \vdots \\ c_{k,\xi} \\ \vdots \\ c_{k,N_{bs}} \end{pmatrix}, \tag{2.58}$$

the equation (2.57) can be rewritten in a matrix form

$$H\Psi_k = \epsilon_k S \Psi_k. \tag{2.59}$$

The electron density $\rho(\mathbf{r})$ is written as the combination of the PW-PW, the PW-AO and AO-AO parts as

$$\rho(\mathbf{r}) = \rho^{PW\_PW}(\mathbf{r}) + \rho^{AO\_PW}(\mathbf{r}) + \sum_j \rho_j^{AO\_AO}(\mathbf{r}). \tag{2.60}$$

The first PW-PW contribution can be calculated conveniently in Fourier space. The PW-AO and AO-AO parts are zero outside the cutoff radius r_c and the inside values can be approximated by their spherical average.
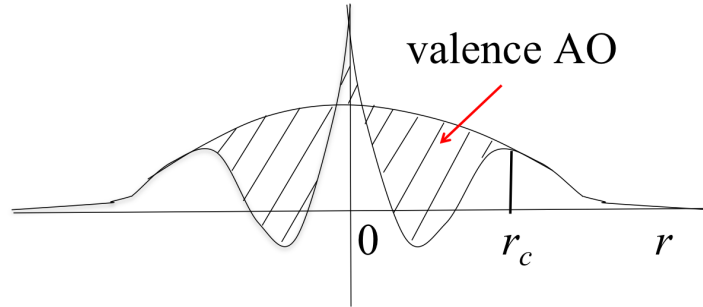

Figure 2.1: All electron mixed basis

The nuclei motion is governed by the Newtonian equation

$$M_I \frac{\mathrm{d}^2 \mathbf{R}_I}{\mathrm{d}t^2} = -\frac{\partial}{\partial \mathbf{R}_I} \left[\langle E_{el} \rangle + \sum_J \frac{Z_I Z_J}{|\mathbf{R}_I - \mathbf{R}_J|} \right], \tag{2.61}$$

where $\langle E_{el} \rangle$ are the expectation value of the electronic part, V_{cl} is the Coulomb potential among nuclei, and $H_{el}(\mathbf{r}, t)$ is the electronic Hamiltonian. $\mathbf{r}$ describes the position of the electrons, while Z_I, M_I, and $\mathbf{R}_I$ denote the atomic number, mass, and the position of nucleus I, respectively. The force acting on nuclei include the Hellmann-Feymanman force as well as the variational force. The all-electron mixed basis approach has many advantages in calculation. First, both extended and localized electronic states can be described very efficiently because both PWs and AOs are used as basis function. Second, a suitable description of core states is possible even in the case of another atom comes close into core regions, if an enough number of PWs is used in basis functions. Third, it take less computer memory in compare with the standard PW approach because there is no need to store the matrix elements between PWs of the Hamiltonian matrix. Fourth but not the last, the matrix element between AOs of two adjacent atoms does not exist since AOs are restricted within non-overlapping atomic spheres. Moreover, in this approach there is no problem of the basis set superposition error (BSSE), and the problem of overcompleteness is reduced.

2.6 Time-dependent GW method

In the TDDFT approach, the explicit density functional of the exchange-correlation energy is unknown, therefore has to be approximated. In the case of ground state simulations, the adiabatic local density approximation (A-LDA) is used for simplicity. On the other hand, for the excited state simulation, we have proposed to use the one-shot GW approximation (GWA) [12, 13, 14, 15]. This is a simple extension of the so-called extended Hartree-Fock approximation for excited states [16]. We have the time-dependent GW (TDGW) quasiparticle equation:

$$i\hbar \frac{\partial}{\partial t} \varphi_i(\mathbf{r}, t) = (T + V_{Hartree} + V_{ext})\varphi_i(\mathbf{r}, t) + \int \Sigma_{ex}(\mathbf{r}, \mathbf{r}', t - t')\varphi_i(\mathbf{r}', t')d\mathbf{r}'dt'. \tag{2.62}$$

Similar with the section 2.4, we use the spectral method to integrate the equation Eq. (2.62).

$$\varphi_i(\mathbf{r}, t + \Delta t) = \sum_k \exp^{-i\epsilon_k^{GW}\Delta t} \left\langle \phi_k^{GW}(\mathbf{r}, t) \middle| \varphi_i(\mathbf{r}, t) \right\rangle \phi_k^{GW}(\mathbf{r}, t), \tag{2.63}$$

where $\phi_k^{GW}(\mathbf{r}, t)$ is the eigenfunction of the H^{GW} which corresponding with the quasiparticle energy ϵ^{QP}. Generally, $\phi_k^{GW}(\mathbf{r}, t)$ is calculated self-consistent with the initial guess as $\phi_k^{LDA}(\mathbf{r}, t)$, however for simplicity one can approximate [48] as

$$\phi_k^{GW}(\mathbf{r}, t) \simeq \phi_k^{LDA}(\mathbf{r}, t), \tag{2.64}$$

then in NAQMD approach, the TDGW equation (2.62) can be integrated as

$$|\varphi_i(\mathbf{r}, t + \Delta t)\rangle \approx \sum_k \exp\left[-\frac{i}{\hbar}\epsilon_k^{GW}(t)\Delta t\right] |\phi_k^{LDA}(\mathbf{r}, t)\rangle \left\{ \left\langle \phi_k^{LDA}(\mathbf{r}, t) \middle| \varphi_i(\mathbf{r}, t) \right\rangle + \Delta t \frac{\partial}{\partial t'} \left\langle \phi_k^{LDA}(\mathbf{r}, t') \middle| \varphi_i(\mathbf{r}, t) \right\rangle_{t'=t} \right\}. \tag{2.65}$$

The detail calculation method of quasiparticle energies is explained in the Appendix B. Here we only present the formula of quasiparticle energy within the one-shot GW approximation

$$\epsilon_n^{GW} \simeq \epsilon_n^{LDA} + \int d\mathbf{r} \int d\mathbf{r}' \phi_n^*(\mathbf{r}) \left[\Sigma_{xc}(\mathbf{r}, \mathbf{r}', \epsilon_n^{GW}) - V_{xc}^{LDA}(\mathbf{r})\delta(\mathbf{r} - \mathbf{r}') \right] \phi_n(\mathbf{r}')$$

$$\simeq \epsilon_n^{LDA} + Z_n \int d\mathbf{r} \int d\mathbf{r}' \phi_n^*(\mathbf{r}) \left[\Sigma_{xc}(\mathbf{r}, \mathbf{r}', \epsilon_n^{LDA}) - V_{xc}^{LDA}(\mathbf{r})\delta(\mathbf{r} - \mathbf{r}') \right] \phi_n(\mathbf{r}'), \tag{2.66}$$

where ϵ_n^{LDA} denotes the corresponding LDA eigenvalue, and Z_n is the renormalization factor defined as

$$Z_n = \left[1 - \frac{\partial}{\partial\omega} \int d\mathbf{r} d\mathbf{r}' \phi_n^*(\mathbf{r}) \Sigma_{xc}(\mathbf{r}, \mathbf{r}', \omega) \phi_n(\mathbf{r}')|_{\omega=\epsilon_n^{LDA}} \right]^{-1}. \tag{2.67}$$

A Successive Hydrogenation Reactions of Carbon Monoxide Producing Methanol

3.1 Introduction

Hydrogenation reaction is a reaction of hydrogen and an other compound or element. Carbon monoxide (CO) is one of the important basic molecules to produce organic compounds. The hydrogenation reaction of carbon monoxide plays an very important role in chemical industry. Normally, the H_2 + CO reaction needs to be carried out using transition metal catalysts. The role of catalysts is unclear and the reaction mechanisms are still on discussing [49]. One of the possible reaction mechanisms is: on the surface of catalyst, hydrogen molecule dissociates into hydrogen atom and then react with CO^- at the surface of catalyst [53]. However, it is difficult to expect the esistence of CO^- in nature because the electron affinity of CO is negative [51]. One of the active catalyst is Nickel[50]. The dissociation pathway of a hydrogen molecule on a nickel dimer was also discovered when a single electron is excited from the HOMO level to the LUMO level by a dynamics simulation in our group [52]. A neutral hydrogen atom may react with a neutral CO without catalyst at excited states.

Methanol is employed primarily as a feedstock for the manufacture of chemicals, and as a fuel for specialised vehicles [54]. It is an useful energy carrier, easy to store in compare with hydrogen and burns cleaner than fossil fuel. Methanol can be produced from the hydrogenation of CO. One of possible reaction

pathways is CO → HCO → H$_2$CO → H$_3$CO → CH$_3$OH. However, the reaction H + H$_2$CO can have another product such as HCO + H$_2$ [55], which are not the favorable intermediates. With the purpose of creating methanol from carbon monoxide, it would be natural to consider the following reactions:

$$H + CO \rightarrow HCO, \tag{3.1a}$$

$$H + HCO \rightarrow H_2CO, \tag{3.1b}$$

$$2H + H_2CO \rightarrow CH_3OH. \tag{3.1c}$$

So far, the reactions of a carbon monoxide molecule with a hydrogen atom have been studied both experimentally and theoretically [56, 57]. One important point is that the first reaction (3.1a) has a barrier height of 4.54 ± 0.14 kcal.mol^{-1} at 0 K [58], so it needs to proceed through an electronic excited state. There were some previous researches focused on the potential energy surface of H + CO reaction at the ground and excited states [59, 60, 61, 62, 63]. These two potential curves cross each other at the transition state of the reaction. Therefore, the most probable first reaction process should be

$$H + CO^* \rightarrow HCO \tag{3.1a'}$$

instead of (3.1a). By carrying out on-the-fly dynamics simulations using TOMBO program, we want to clarify the reaction pathway of producing methanol from carbon monoxide at the atomic level.

3.2   Initial condition

The methodology of *ab inito* molecular dynamics based on the time-dependent density functional theory (TDDFT) or the time-dependent GW (TDGW) method of TOMBO program was explained in Chapter 2 , Section 2.4, 2.5, 2.6. In the simulation, first, the initial electronic states are determined self-consistently at a given electronic configuration before the time-dependent simulation starts. Second, the TDDFT or TDGW simulation starts after the initial electronic states are determined. The Hamiltonian is expected to change only very slightly in the time Δt= 0.1 fs. Following the Franck-Condon approximation [64], the excited simulation is initiated by vertical excitation of one up-spin electron from the HOMO level to

the LUMO level. The number of up-spin electrons and down-spin electrons are kept constant during the simulation.

A simple cubic unit cell of 10 Å for the reaction (3.1b) and 12 Å for the reaction (3.1c) was used. The cutoff energy for PWs is set at 18 Ry (1 Ry = 13.6 eV), which is enough to obtain the optimized structure for a system with hydrogen atoms. Matrix diagonalization is used not only for the initial self-consistent field (SCF) loop to get good convergence of the electronic states but also during the TDDFT dynamics. $100 - 800$ levels are used in the spectral decomposition (2.50). In the GWA calculation for the reaction (3.1a'), fcc unit cell of 15 Å is used where the Coulomb interaction is spherically cut to avoid interactions with adjacent unit cells, and the cutoff energies corresponding to 44 Ry and 7 Ry are set, respectively, for the exchange and correlation parts of the self-energy. The cutoff energy for PWs is set at 14 Ry.

For the ground state simulation of the H + CO reaction, several values of the initial velocity is given for H atom. In all other cases, the initial velocity of each atom is set at 0. All molecules' geometrical structure at the initial time is set as their optimized structure by TOMBO program. The position of hydrogen atoms is set at some different places to find the suitable one leading to the expected reaction (the reactions (3.1a'), (3.1b) and (3.1c)).

3.3   Results and Discussion

3.3.1   The H + CO reaction

We start the simulation of H + CO from the initial configuration shown in Fig. 3.1. The optimized bond-

Figure 3.1: Initial geometry of H + CO reaction.

length of CO by TOMBO is 1.178 Å. The initial distance between C and H and the initial H-O-C angle are set at 2.06 Å and 150.945°, respectively. First we performed the reaction with the initial velocity of

each atom equal to 0. There reaction does not happen during the ground state simulation if the hydrogen molecule has small velocity. Fig. 3.2 shows the distance between carbon and hydrogen atoms during the ground state simulation with zero initial velocity. At first, the H atom approaches the CO molecule slightly, and then is repelled and oscillates near the C atom. As intermediate trajectory, Fig. 3.3 presents the snapshot of the simulation at every 10fs. This result does not change even if we use the GWA. The energy conservation requirement is fulfilled in our simulation, if the nuclear kinetic energy is added to the total energy.
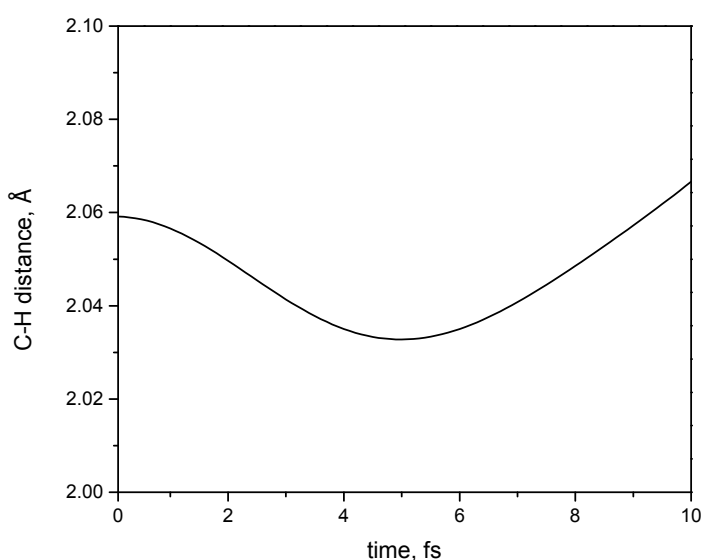
Figure 3.2: The distance between carbon and hydrogen atoms in the ground state simulation of H + CO, in the case the initial velocity of H atom is 0.

If the H atom has a certain initial velocity, the reaction can only happen at a very high value of velocity; see Fig. 3.4. The reaction takes place if the initial kinetic energy is equal to or greater than 5 eV. This is presumably because the electronic state is different and it is not so easy to convert the nuclear kinetic energy to the electron excitation energy in the system. The result helps to confirm what we have mentioned before: without catalyst and the small initial velocity of hydrogen, the reaction H + CO can not happen at ground state.
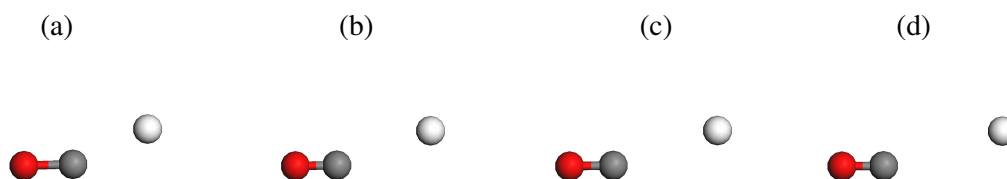
Figure 3.3: Snapshots of H + CO at ground state simulation with the initial velocity of hydrogen atom $v = 0.0018m/fs$: (a) 10 fs, (b) 20 fs, (c) 30 fs, (d) 40fs
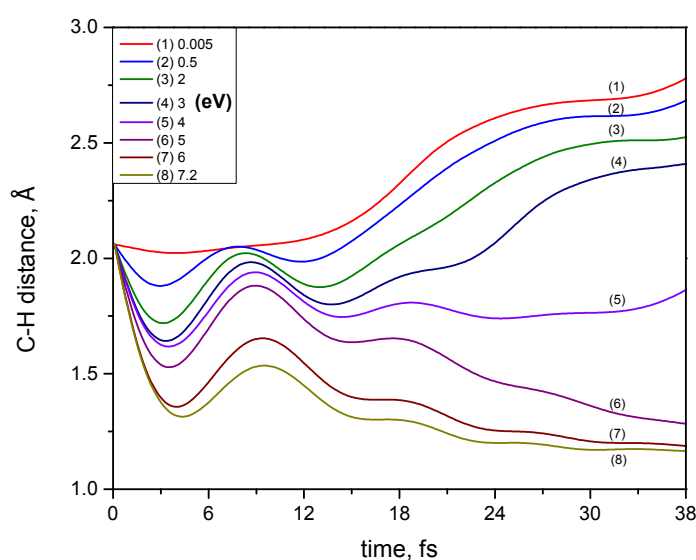
Figure 3.4: C-H distances by initial kinetic energies of H atom. The unit of kinetic energies is eV. The reaction can not happen if the initial kinetic energy smaller than 4 eV.

3.3.2 The H + CO* reaction

As the next step of the simulation, we perform the excited state simulation, where one up-spin electron is excited from the HOMO level to the LUMO level. Instead of the LDA, we have applied the GWA for the exchange correlation energy to solve Eq.(2.44). The hydrogen atom approaches to the carbon monoxide, and after 20 fs, a HCO molecule is produced, although a vibration remains in the C-O bond.

Fig. 3.5 (a) shows the distance between carbon and hydrogen atoms during the excited state simulation. The C-H distance has decreased from 2.1 Å to 1.24 Å at 20 fs, forming C-H bond. Then, there is only small change (reducing by 0.15 Å from 20 fs to 50 fs) in the C-H bond length. Fig. 3.5 (b) shows the time evolution of the up-spin quasiparticle energies. Red solid and dashed curves correspond, respectively, to the original LUMO (now occupied) and to the original HOMO (now unoccupied). Note that the order of these two levels is interchanged due to the Fock exchange interaction, which shifts up (down) the quasiparticle energies of the unoccupied (occupied) levels. The HOMO and LUMO energies of CO* (at 0 fs) and HCO (at 40 fs and 70 fs) are presented in Table 3.1. According to the reference data [65], the HOMO (original LUMO) energy of CO* is 8.0 eV, which is equal to the ionization potential (IP) of 14.0139 eV minus the first photoabsorption energy of 6.036 eV of CO. For HCO, the IP and the electron affinity (EA) are 8.14 ± 0.04 eV [66] and 0.3130 ± 0.04 eV [67], respectively. These reference data are comparable to the values listed in the table if we take the average over the later times, which indicate the validity of the present time-dependent GW (TDGW) approach.

Table 3.1: HOMO and LUMO energies in the H + CO* reaction. HOMO and LUMO denote, respectively, the red solid curve and the red dashed curve in Fig. 3.5 (c).

	HOMO (eV)	LUMO (eV)
CO* (at 0 fs)	- 9	- 3
	(original LUMO)	(original HOMO)
CO* (Reference)	- 8 [65]	-
HCO (at 40 fs)	- 12	- 1
HCO (at 70 fs)	- 7	2
HCO (Reference)	- 8.1 [66]	0.3 [67]

3.3.3   The H + HCO reaction

The next step is adding one more hydrogen atom to the HCO molecule. We start the ground state simulation from the initial configuration given in Fig. 3.6. The H-C, C-O bond lengths and the H-C-O angle in the optimized HCO molecule are 1.14 Å, 1.21 Å and 123.8°, respectively. Another H atom is put on the same plane, where the distance between C and H is set at 1.75 Å and the H-C-H angle is 89.8°.
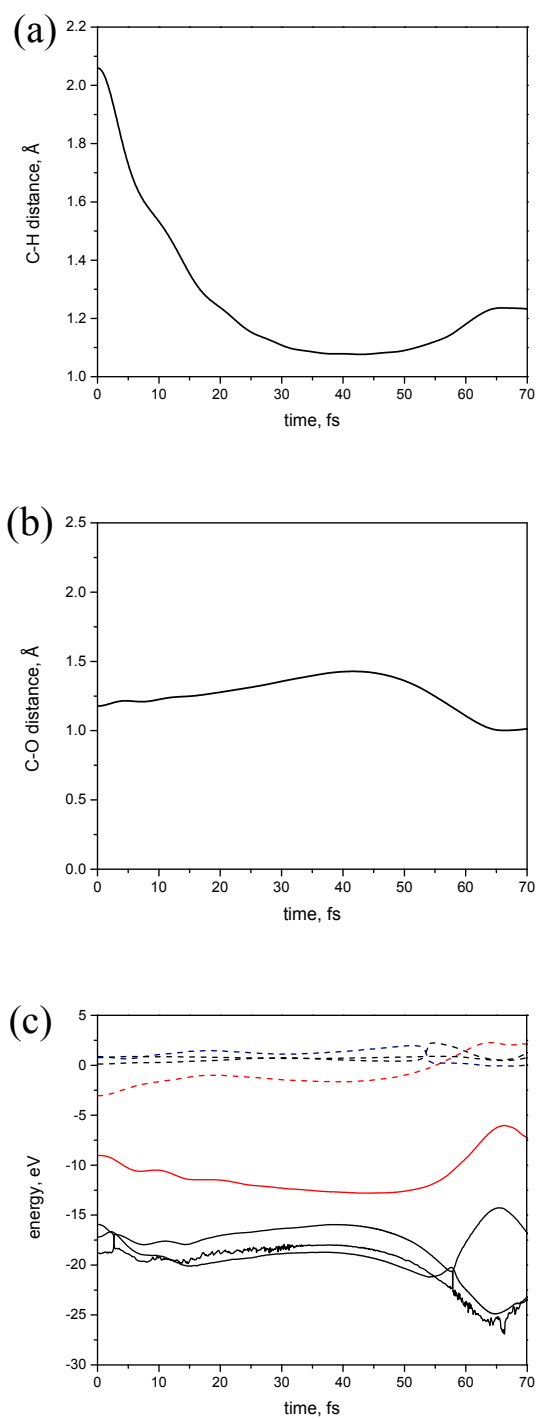
Figure 3.5: (a), (b) The distances between carbon and hydrogen atoms and between carbon and oxygen atoms, respectively, in the H +CO reaction. The reaction trajectory, where hydrogen atom approaches to carbon atom, is observed. (b) The time evolution of the up-spin *GW* quasiparticle energies (in unit of eV), where the occupied levels are solid lines and the unoccupied levels are dashed lines. Red solid and dashed curves correspond, respectively, to the original LUMO (now occupied) and to the original HOMO (now unoccupied).
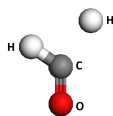
Figure 3.6: Initial geometry of H + HCO reaction.

The C-H distance has decreased by 0.71 Å during 8 fs of simulation, the hydrogen atom approaches easily to the HCO molecule to form a H_2CO molecule at 6 fs, see Fig. 3.7(a). The HOMO and LUMO levels are kept almost the same during the simulation, while the LUMO + 1 level goes up and the HOMO - 2 levels goes down forming the new electronic state of H_2CO as shown in Fig. 3.7(b).

3.3.4 The 2H + H_2CO reaction

As mentioned before, the reaction H + H_2CO can have another product such as HCO + H_2 [55], which are not the favorable intermediates. Therefore, we included two H atoms in this simulation. It is difficult to scan the hole potential energy surface of the system, so we did some trials to find the proper initial position of two hydrogen atoms. One of the good candidate for the initial configuration of the ground state simulation is shown in Fig. 3.8 and Table 3.2. An other initial configuration was presented in our paper [24], in which the $\angle COH2 = 90°$. If the distance of hydrogen atoms to carbon and oxygen atom are 1.8 Å respectively, the reaction did not happen. The two almost isolated H atoms are initially separated at 3.904 Å , which is considered as a suitable distance to be regarded as two separated H atoms.
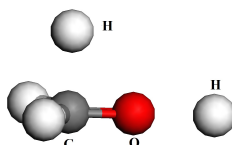
Figure 3.8: Initial geometry of 2H + H_2CO reaction.

Fig.3.9 shows the time evolution of the distance between carbon, oxygen and hydrogen atoms and the time evolution of the Kohn-Sham energy expectation values of the up-spin electron in the (3.1c) reaction. Both C-H distance and O-H distance have decreased during the simulation. In first 10 fs, the O-H distance
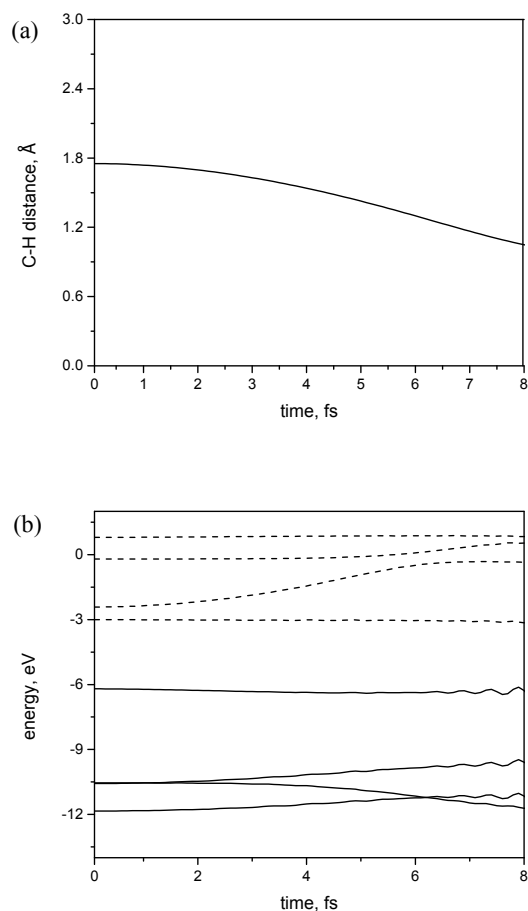
Figure 3.7: (a) The distance between carbon and hydrogen atoms in the reaction H + HCO. (b) The time evolution of the Kohn-Sham energy expectation values (in units of eV), where the occupied levels are solid lines and the unoccupied levels are dashed lines.

has reduced to 1.191 Å while the C-H distance has decreased by only 0.138 Å. The HOMO level goes down while the LUMO levels goes up to the new electronic state of CH$_3$OH.

Fig. 3.10 shows the snapshot of the simulation as the intermediate trajectory of the hydrogenation of carbon monoxide reaction.

Tabel 3.3 compares of the interatomic distances and angles of the product molecules at the final time step of the simulation with experimental data [68, 69, 70]. There are nonnegligible differences between
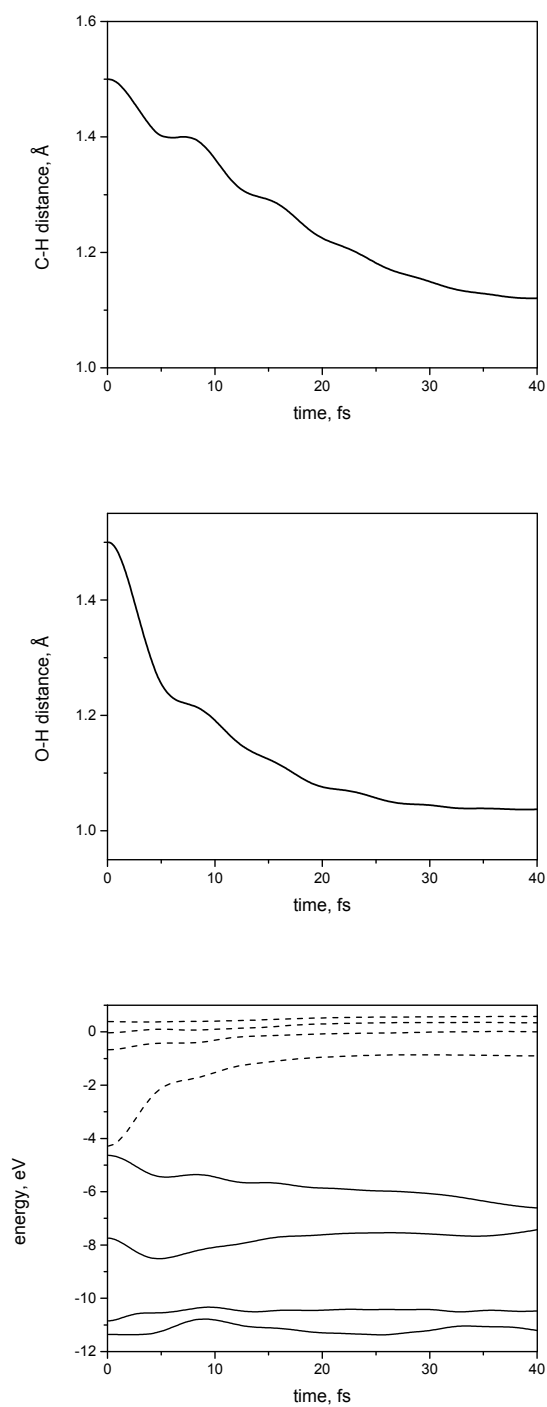
Figure 3.9: The distances between (a) carbon and hydrogen atoms, and (b) between oxygen and hydrogen atoms, in the reaction 2H + H_2CO. (c) The time evolution of the Kohn-Sham energy expectation values (in units of eV), where the occupied and unoccupied levels are drawn by solid lines and dashed lines, respectively.

Table 3.2: Interatomic distances and angles at initial stage of the reaction 2H + H$_2$CO.

		Initial geometry
H$_2$CO	C-O	1.207 Å
	C-H	1.110 Å
	∠OCH	122.44°
	∠HCH	115.30°
	C-H1	1.5 Å
	O-H2	1.5 Å
	H1-H2	2.4 Å
	∠OCH1	90°
	∠COH2	180°

(1) (a)   (b)   (c)   (d)

(2) (a)   (b)   (c)   (d)

(3) (a)   (b)   (c)   (d)
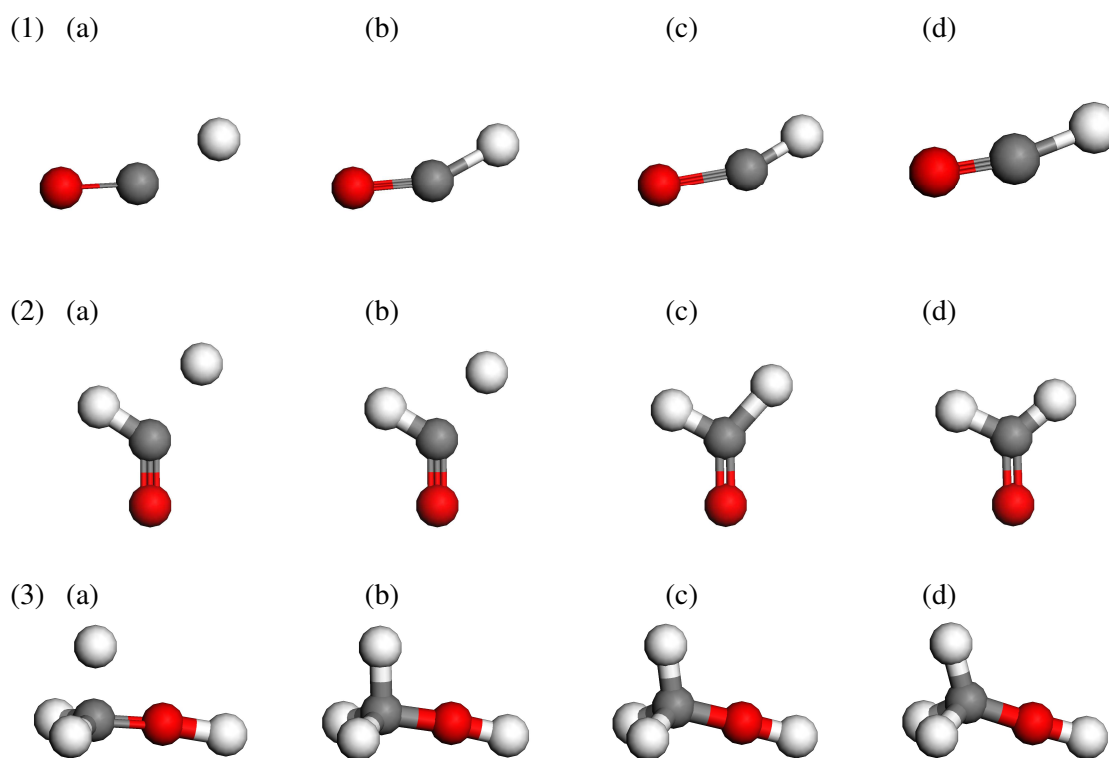
Figure 3.10: (1) Snapshots of H + CO reaction yielding HCO: (a) 10fs, (b) 20 fs, (c) 40 fs, (d) 60 fs. (2) Snapshots of 2H + H$_2$CO → H$_3$COH: (a) 10 fs, (b) 20 fs, (c) 30 fs, (d) 40fs. (3) Snapshots of 2H + H$_2$CO → H$_3$COH: (a) 10 fs, (b) 20 fs, (c) 30 fs, (d) 40fs.

the simulation results and the experimental data. However, the products at the final step have not yet been at the stable ground state, so that these differences can be considered within acceptable tolerance.

Table 3.3: Interatomic distances and angles of the product molecules at the final time step compared with experimental data [68, 69, 70].

		CAL	EXP	error
HCO	C-O	1.361 Å	1.175 Å[a]	15.8 %
	C-H	1.09 Å	1.125 Å[a]	3.1 %
	∠OCH	162.89°	124.95°[a]	30.36 %
H_2CO	C-O	1.262 Å	1.205 Å[b]	4.7 %
	C-H	1.050 Å	1.113 Å[b]	5.6 %
	∠OCH	128.44°	121.90°[b]	5.4 %
	∠HCH	115.11°	116.13°[b]	0.9 %
CH_3OH	C-O	1.3 Å	1.427 Å[c]	8.8 %
	O-H	1.037 Å	0.956 Å[c]	8.8 %
	C-H	1.121 Å	1.096 Å[c]	2.3 %
	∠OCH	123.557°	108.87°[c]	13.5 %
	∠COH	176.891°	108.52°[c]	63 %
	∠HCH	105.027°	109.03°[c]	3.7 %

[a] See Ref.[68]. [b] See Ref.[69]. [c] See Ref.[70].

3.3.5 Remark on a Quantum Fluctuation Effect

In the simulation of $H + CO$ reaction, we have ignored the quantum mechanical fluctuations of hydrogen atoms. This is of course an approximation, but can be considered as not so bad approximation except for the first ground-state simulation of $H + CO$, where the H atom does not react with the CO molecule. In this case, the adiabatic potential surface for the H atom is very flat and the nuclear wave function of the H atom will become very broad. Therefore, even though our conclusion that H does not react with CO does not change, our treatment ignoring the quantum mechanical nature of the H atom should be regarded as a rough approximation. On the other hand, in the excited state simulation of H + CO, the H atom spontaneously approaches to the CO molecule to form the HCO product. The trajectory clearly shows that the H atom sliding down a downhill of the (excited state) adiabatic surface. In such a case, even if we take account of the quantum fluctuations, the trajectory movement is expected not to change significantly.

Similar situation happens in the H + HCO reaction. In the last simulation of 2H + H$_2$CO, the existence of two hydrogen atoms nearby H$_2$CO clearly makes the reaction easier to occur, because we could not succeed in the one-by-one addition of H atoms onto H$_2$CO. Obviously there is no energy barrier and no activation energy is required to induce this 2H reaction. The two H atoms spontaneously approach to the H$_2$CO molecule as if they slide down a downhill. Therefore, we expect that our result does not change significantly even if we introduce the effect of the quantum fluctuations of the H atoms in this case also.

Photochemical ring opening of oxirane: An all-electron first-principles study

4.1 Introduction

In this Chapter, we consider the photochemical ring opening reaction of an oxirane molecule (C_2H_4O). Oxirane is the simplest epoxide with a three-membered ring consisting of one oxygen atom and two carbon atoms. It easily participates in addiction reactions, opens its ring and thus easily polymerizing. The ring-opening reaction of oxirane is very important to study other electrocyclic reaction, for example ring-opening reaction of vitamin D. It is believed that this reaction happens around the crossing region between the energy levels [71]. Oxirane is a small molecule where the photochemistry is expected to be applicable for MD based on TDDFT simulation and provides a simple prototype for investigation of more complicated photochemical reactions [71]. Tapavicza et al. [72] have performed a mixed quantum/classical trajectory surface-hopping (TSH) of asymmetric ring opening of oxirane and found that several states are involved in mediating the ring-opening reaction. Jian-Hao Li et al. [73] analyzed the behavior of the first few low-lying excitations of oxirane molecule by performing a TDDFT calculation followed by the quantified natural transition orbital (QNTO) analysis. However, based on the stochastic nature of the surface-hopping approach, the results is dependent on the initial chosen trajectories and takes an expensive computational cost. It is important to find out which electronic states are responsible for the reaction (as

well as why these states are responsible). Therefore, it would be interesting to perform the excited state dynamics simulation by using TOMBO programs.

In order to perform an ab initio MD simulation at some first excited states, it is better to know which level would be the good candidate for the ring opening of oxirane molecule. In this sense, the optical absorption spectra that includes the information the electronic transition between one-particle energy levels is required. First we calculate the optical spectra of oxirane by using the GW + Bethe-Salpeter equation (BSE) method [74, 75, 76, 77, 78]. In this method, the electron-hole (two-particle) Green's function including the ladder diagrams up to the infinite order within the GW approximation (GWA) is calculated. The GW + Bethe-Salpeter method has been applied to various molecules, clusters, semi-conductors, and etc... to calculate their optical absorption spectra, although it has been recently suggested that it significantly underestimates the optical gap in particular for small molecule [79]. Then we perform the excited-state dynamics simulations by using the NAQMD method based on the ALDA. With the new implementation of TDGW approach in TOMBO code, we have also performed the TDGW simulation for the first three excited states of oxirane molecule.

4.2   Methodology

4.2.1 GW + Bethe-Salpeter method

In this subsection, we are going to explain very briefly the GW+BSE formalism, the detail of this method can be found in many papers [74, 75, 76, 77, 78]. The GW + Bethe-Salpeter calculation can be derived basically in the next two steps. In the first step, the GW calculation [13, 14, 15, 12, 81, 80] is applied to estimate the accurate quasiparticle energies including the first ionization potential and the electron affinity. In the second step, the Coulomb interaction between the electron and the hole generated in the occupied state is considered by the BSE and its eigenvalue problem is solved. The coupling part bridging between the resonant part and anti-resonant part are neglected by using the Tamm-Dancoff approximation [82]. Then the kernel in the BSE is written as $\Xi \simeq -U^{ex} + W^d$, here U^{ex} is a bare Coulomb interaction corresponding to the exchange term which comes from the Hartree term in the self-energy and W^d is a dynamically screened Coulomb interaction corresponding to the direct term which comes from the GW

self-energy (the second-order exchange term $G\frac{\partial W}{\partial G}$ is small [83, 84] so that it can be neglected). The similar formulation is given in [74, 75] by using pseudopotentials.

A many body perturbation theory, in general, is based on the Green function which requires summing over very large number of empty states. The plane waves (PW) basis set can most accurately describe the empty states. To accurately describe the electrons in the core region, on the other hand, the atomic orbital (AO) basis set is known to work well compared to the PW basis set. The all-electron mixed basis approach, using PWs and AOs in a combined way [85, 86, 87] is able to meet the both requirements.

We use an fcc supercell of size of 15 Å . The cut-off energy of the PWs is 17.7 Ry (1 Ry = 13.6 eV). The Coulomb interaction is spherically cut to avoid interactions with adjacent unit cells, and the cutoff energies corresponding to 63.7 Ry and 11.0 Ry are set, respectively, for the exchange and correlation parts of the self-energy. 4000 levels are used in the summation deriving the polarization function and the GW self-energy, and 200 empty levels are used to solve the Bethe-Salpeter equation. These parameters are sufficient to get a well converged LDA Kohn-Sham orbital energies and *GW* quasiparticle energies, in particular, at HOMO and LUMO levels.

4.2.2   Molecular dynamics based on time-dependent density functional theory

Our method of *ab inito* molecular dynamics based on time-dependent density functional theory (TDDFT) was explained in the section 2.4. We use a simple cubic unit cell of 12 Å for the simulation. We use minimal AOs, which have finite values only within each nonoverlapping atomic sphere. AOs are smoothly truncated by subtracting a smooth quadratic function, which has the same amplitude and derivative at the atomic sphere surface [18]. This quadratic function smoothly connecting to the tail of the true AO can be successfully described by a linear combination of PWs. The cutoff energy for PWs are set at 17.27 Ry ($1Ry = 13.6eV$). Matrix diagonalization is used not only for the initial self-consistent field (SCF) loop to get good convergence of the electronic states but also during the TDDFT dynamics.

Equation (2.45) is the usual Newtonian equation of motion coupled with the force quantum mechanically calculated as the negative gradient of the total energy. We use a vibrational force for the derivative of the total energy, as formulated by Ho et all. [47].

Our TDDFT or TDGW treatment involves the following two steps: First, the initial electronic states

are determined self-consistently at a given electronic configuration before the time-dependent simulation starts. Second, the TDDFT/TDGW simulation starts after the initial electronic states are determined. Equation (2.51) (for nonadiabatic simulation) is used stepwise in $\Delta t = 0.05\,fs$ interval where the Hamiltonian is not expected to change.

Our simulation is restricted to reactions initiated in the third lowest excited states. This conditions are based on the photolysis experiment of Kawasaki *et al.* [88] since the experimental photoabsorption energies (0.67-6.95 and 7.11 eV) may populate only the lowest excited states of oxirane [72]. Following the Franck-Condon approximation [64], the first S_1, second S_2 and third S_3 excited state simulations are initiated by vertical excitation one up-spin electron from HOMO level to LUMO level, to LUMO +1 level, and to LUMO +2 level, respectively. The number of up-spin electrons and down-spin electrons are kept constant. The initial velocity of each atom is set at 0 in all cases.

4.3 Results and Discussion

4.3.1 Optical spectra of oxirane

The first step of our study is to determine the initial structure of oxirane molecule (Fig. 4.1) by the optimization of the geometry of the gas phase molecule. The calculated results are compared in Table 4.1 with the known experimental values [89]. It is seen that the LDA optimized geometry by TOMBO is in a good agreement with the experimental data.
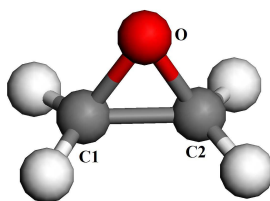

Figure 4.1: Initial geometry of oxirane

The photoabsorption spectra of oxirane are presented in Fig. 4.2 and the level-to-level contributions (in %) to the first three photoabsorption states are listed in Table. 4.3. The first photoabsorbed state has a main

Table 4.1: Interatomic distances and angles of oxirane at initial stage compared with the experimental data [89].

	Initial geometry	References [89]
C-O	1.41 Å	1.43 Å
C-H	1.10 Å	1.09 Å
∠C1OC2	62.5°	61.62°
∠HCH	115.97°	116.9°

contribution (40.5 %) from HOMO → LUMO+2 (corresponding to S_3) and not visible in Fig. 4.2. The transition from the HOMO level to the LUMO level (S_1) mainly contributes to the second photoabsorption state (about 53.6 % in Tabel. 4.3).
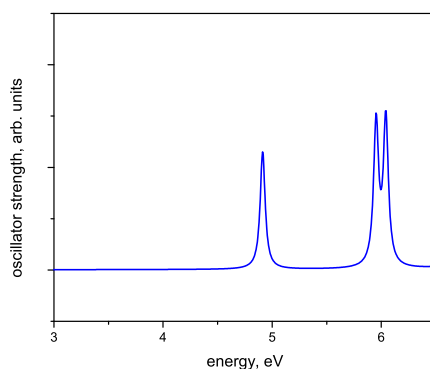
Figure 4.2: Photoabsorption spectra calculated for oxirane.

4.3.2 Photochemical ring opening of oxirane

The Kohn-Sham wave packets is presented in Fig. 4.3. The results was presented together with the orbitals obtained using the LDA and PBE functional in CASTEP program. One can easily see the similar shape of these orbitals.

The TDDFT dynamics simulation's results of the first excited state S_1 are shown in Fig.4.4 and 4.5. Figure 4.4 represents the intermediate trajectory, snapshot were taken at 30fs, 50fs, 60fs, 70fs and 90 fs.

Table 4.2: HOMO-LUMO gap and the ionzation potential energy (IP-based on Koopmans' theorem, in eV) are calculated by the LDA and the GWA using the all-electron mixed basis (TOMBO). Our results are compared with the calculated reference data by other methods using the 6-31G* basis set and the available experimental data [90].

		HOMO-LUMO gap	IP
TOMBO	LDA	5.94	6.6
	GWA	11.16	10.89
Cal. [90]	HF	18.89	12.12
	LSDA	7.5	6.40
	B3LYP	10.13	7.27
	PBEPBE	7.69	5.79
	CID	18.89	12.14
Expt. [90]|	–	–	10.57

Table 4.3: Level-to-level contributions (in %) to the first three photoabsorption states in the single transition.

First		Second		Third	
4.91 eV		5.95 eV		6.04 eV	
12→15	40.5 %	12→13	53.6 %	11→13	2.2 %
12→17	2.1 %	12→17	30.1 %	11→15	36.3 %
12→21	1.1 %	–		11→17	8.4 %
12→22	5.8 %	–		11→22	8.2 %
12→25	10.9 %	–		11→25	9.5 %
12→29	3.5 %	–		11→28	1.2 %
12→48	5.0 %	–		11→29	3.7 %
12→66	1.9 %	–		11→66	1.7 %
12→68	1.1 %	–		11→72	2.6 %
12→72	5.3 %	–		–	

The reaction does not occur during the first 50 fs. Around the 50 fs, the HOMO (unoccupied) level goes up while the LUMO level (occupied) goes down rapidly. Then a crossing between two levels occurs around 80 fs, see Fig. 4.5 (c). The change of electronic level makes change in molecule geometry respectively. One can see in Fig. 4.5, the C1-O bond length decreases while the C2-O bond length increases. However, The CCO ring was started opening around 70 fs, even before the point of level crossing (around 80fs).

Next we performed the TDDFT dynamics simulation of the second excited state S_2. In this case, one
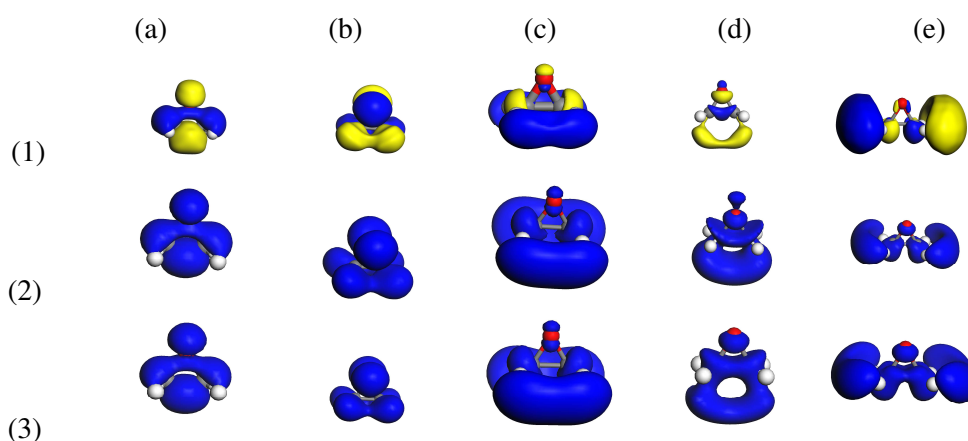
Figure 4.3: (Color online) Ground-state orbitals: (1) using the LDA functional in TOMBO (The blue and yellow indicate regions where the wave function has negative and positive values, respectively), (2) using the LDA functional in CASTEP program, (3) using PBE functional in CASTEP program; (a) HOMO -1 level, (b) HOMO level, (c) LUMO level, (d) LUMO+1 level, and (e) LUMO + 2 level.
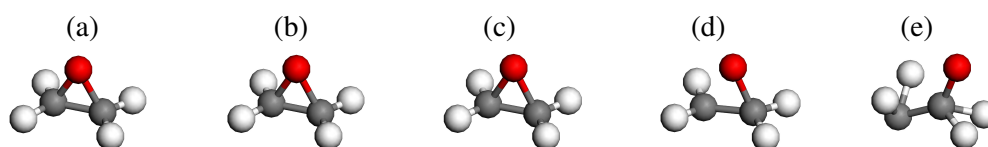

Figure 4.4: Snapshots of the photochemical ring opening of oxirane molecule at the first excited state S_1 simulation using TDDFT: (a) 30 fs, (b) 50 fs, (c) 60 fs, (d) 70fs, and (e) 90 fs.

up-spin electron was excited from the HOMO level to the LUMO + 1 level. As the intermediate trajectory, snapshots at every 10 fs (after 20fs) are shown in Fig. 4.6. Comparing the Kohn-Sham eigenvalue energy levels in Fig. 4.7 (c) in the second excited state simulation and the respectively one in Fig. 4.5 (c), one can easily see that there is small change in all energy levels. In particularly, the LUMO+1 (occupied) level and the LUMO (unoccupied) level are very close to each other and the level crossing occur between these levels around the early time of simulation. After that, the LUMO +1 level goes up and the crossing with the LUMO+2 level occurs around 30 fs, lead to the rapid opening of CO ring. Our result is consistent with the previous Tully's fewest switches surface hopping molecular dynamics (TFSH) [72] and the analysis of potential energy surface of Jian-Hao Li et al. [73], that both agreed that the second excited state would lead to a rapid ring opening reaction. The reaction pathway validate the Gomer-Noyes mechanism of
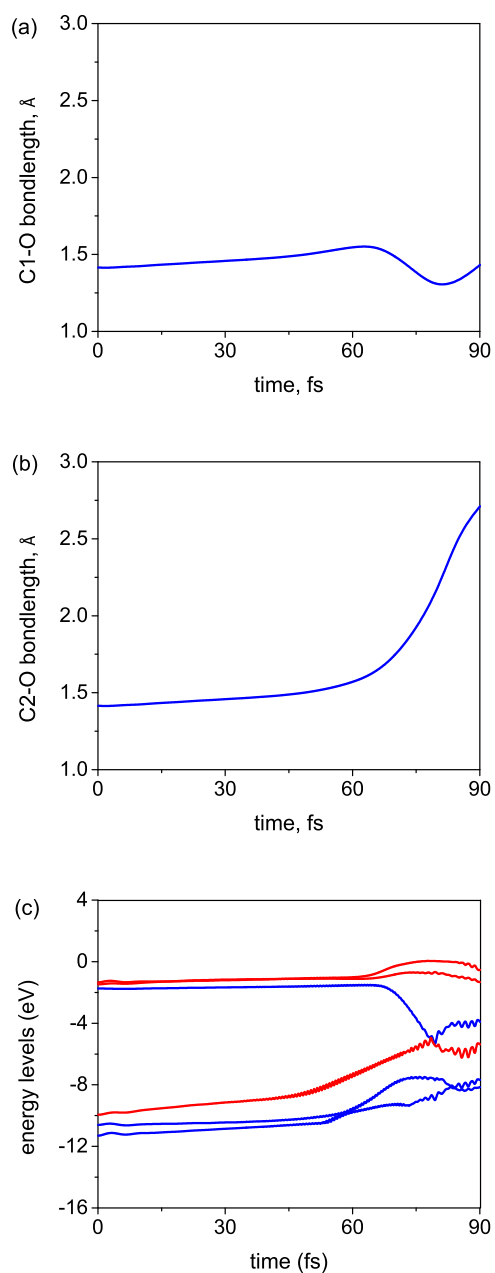
Figure 4.5: The TDDFT result of the first excited state S_1: The time involution of interatomic bond length: (a) The distance between C1 and O. (b) The distance between C2 and O. (c) The time evolution of the Kohn-Sham eigenvalues, respectively, where the occupied levels are blue and the unoccupied levels are red.
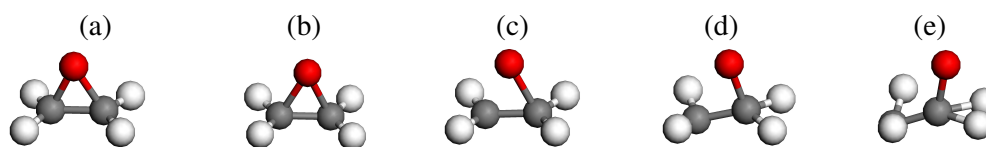
Figure 4.6: Snapshots of the photochemical ring opening of oxirane molecule at the second excited state S_2 simulation using TDDFT: (a) 20 fs, (b) 30 fs, (c) 40 fs, (d) 50fs, and (e) 60 fs.

photochemical ring opening of oxirane, which was derived exprimentally [91].

The TDDFT dynamics simulation of the third excited state S_3, in which one up-spin electron was excited from the HOMO level to the LUMO + 2 level, is also performed. As the intermediate trajectory, snapshots at 20 fs, 40 fs, 80 fs, 100 fs and 150 fs are shown in Fig. 4.8. It is interesting to see that for the third excited state, the LUMO (unoccupied) level, the LUMO + 1 (unoccupied) level and the LUMO + 2 level are very close to each other. It might be the reason for small vibration in all energy levels, see Fig. 4.9 (c). The reaction did not happen until 125 fs, where there is a crossing between the LUMO +1 and the LUMO + 2 levels. However, in this case the C1-O bond breaks in contract with the C2-O bond break in the case of the first and second excited sates simulation, see Fig. 4.9 (a), (b). Our results is in a good agreement with Jian-Hao Li et al. [73] which proposed that the reaction would be more difficult at the third excited state.

We have also performed the TDGW simulation for the first three lowest excited state. Fig. 4.10 presents the time evolution of two C-O bondlength in the C-O-C ring of oxirane. Because of the time consuming, we have not reach to 150 fs of the third excited state simulation. However, the TDGW simulation also found that the second excited state would lead to the rapid CO ring opening, which in in agree with previous studies and help to confirm the NAQMD simulation. Fig. 4.11 shows the time evolution of the quasiparticle energy in the three excited states simulation. The crossing between occupied level and unoccupied level happen around 50 fs for the second excited state simulation, and for the first excited it happens around 75 fs. The snapshots of the three excited states S_1, S_2 and S_3 simulation using TDGW was shown in Fig. 4.12 One can see that in the TDGW simulation, for the first excited state at the C1-O bondlength increase while the C2-O bondlength decrease around 70 fs but the bond does not break at this point, see the green line in Fig. 4.12 (a) and (b). This result is different with the TDDFT simulation,
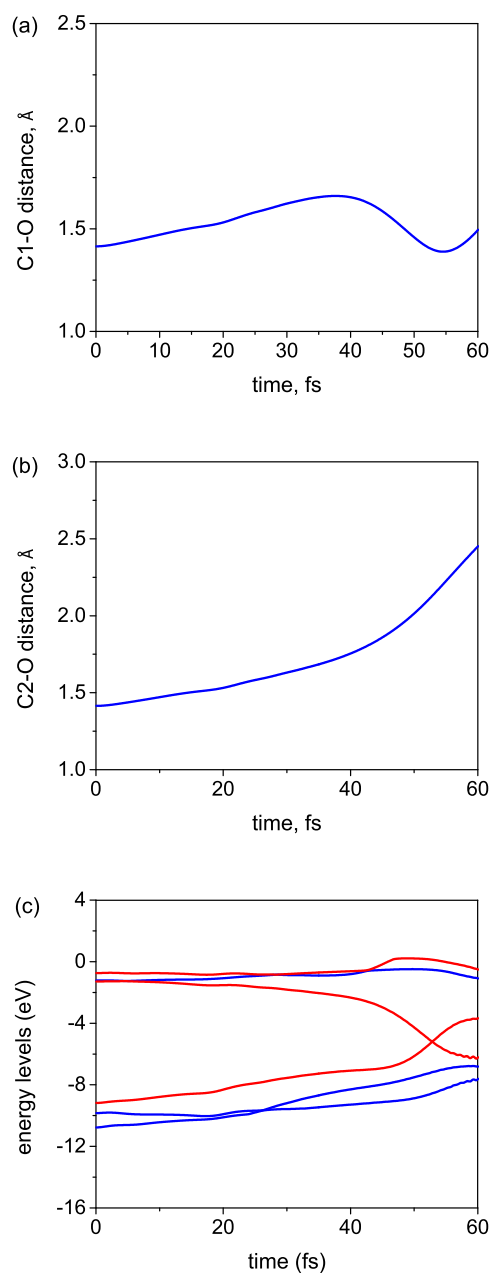
Figure 4.7: The TDDFT result of the second excited state S_2 simulation: The time involution of interatomic bond length: (a) The distance between C1 and O. (b) The distance between C2 and O. (c) The time evolution of the Kohn-Sham eigenvalues, where the occupied levels are blue and the unoccupied levels are red.
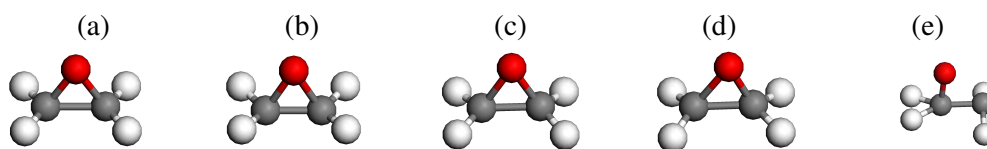
(a) (b) (c) (d) (e)

Figure 4.8: Snapshots of the photochemical ring opening of oxirane molecule at the third excited state S_3 simulation using TDDFT: (a) 20 fs, (b) 40 fs, (c) 80 fs, (d) 100fs, and (e) 150 fs.

which the C1-O bondlength breaks around 70 fs, see Fig. 4.4. Comparing the Kohn-Sham eigennergies and the quasiparticle energies of HOMO and LUMO level, the crossing point between two levels happen at different time step, see Fig. 4.13. The TDGW result is more accurate than the TDDFT result because the change of molecular geometry follow immediately with the level crossing.
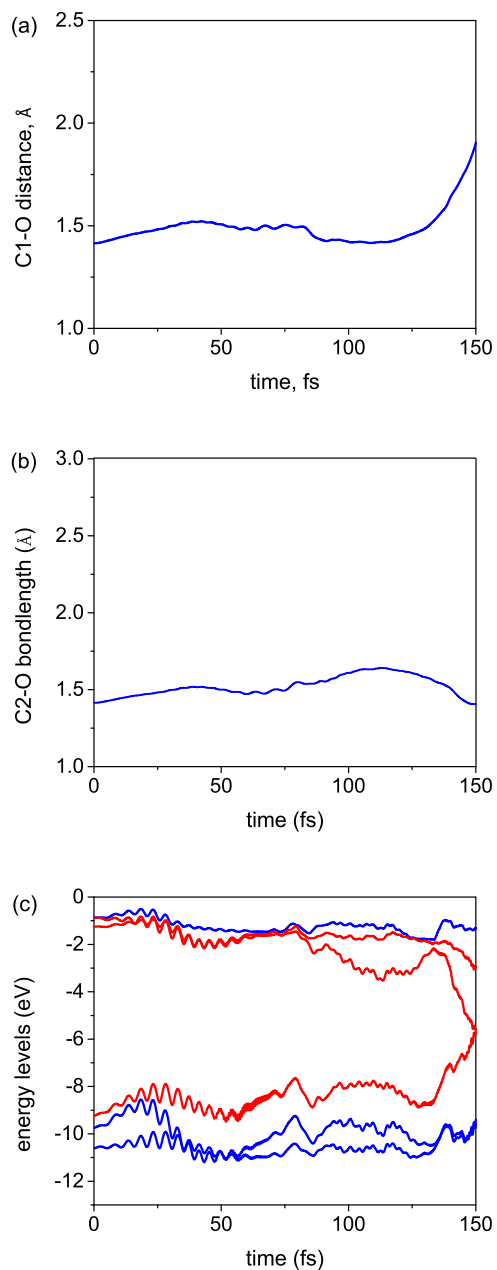
Figure 4.9: The TDDFT result of the third excited state S_3 simulation's result: The time involution of interatomic bond length: (a) The distance between C1 and O. (b) The distance between C2 and O. (c) The time evolution of the Kohn-Sham eigenvalues, where the occupied levels are blue and the unoccupied levels are red.
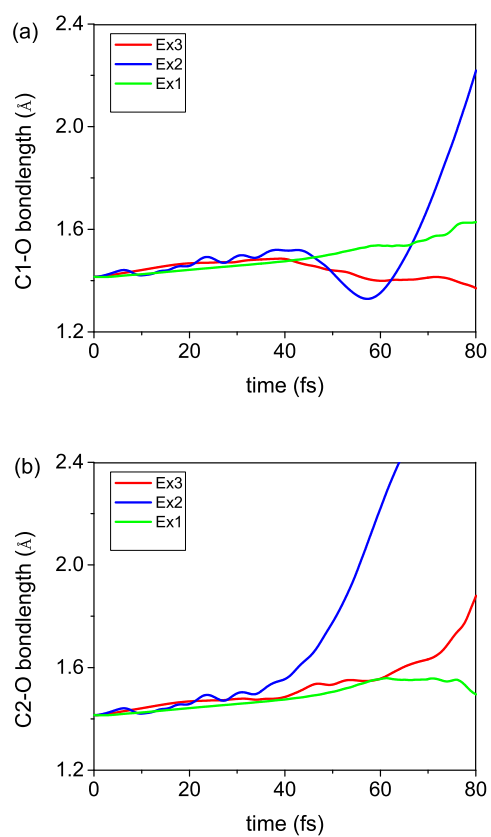
Figure 4.10: The time evolution of the two C-O bondlength in C-O-C ring of oxirane molecule in the first S_1 (green line), second S_2 (blue line) and third S_3 (red line) using TDGW: (a) The distance between C1 and O. (b) The distance between C2 and O.
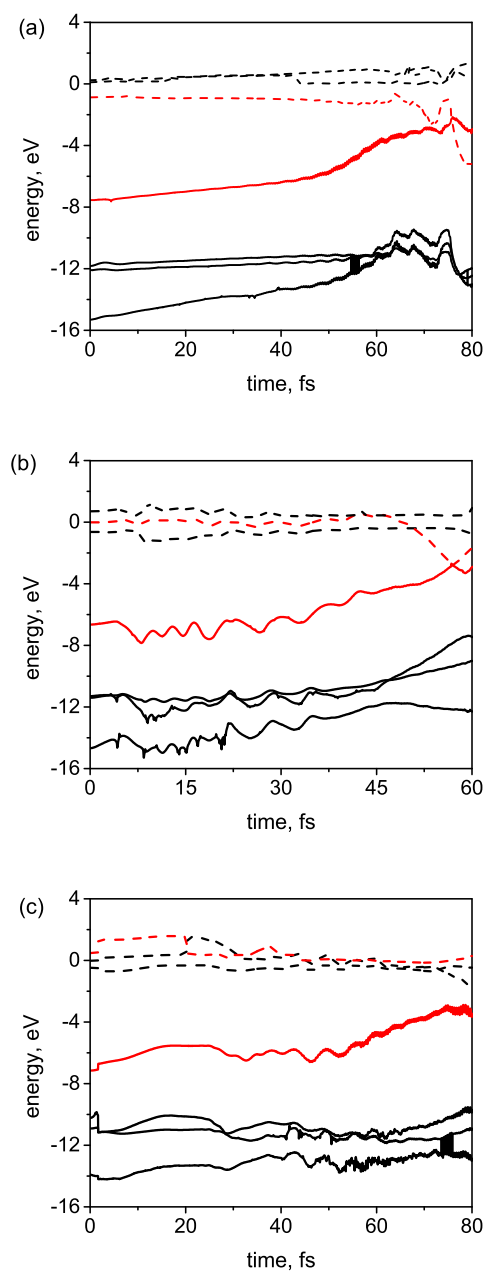
Figure 4.11: The time evolution of of the up-spin *GW* quasiparticle energy (in units of eV), where the occupied and unoccupied levels are drawn by solid lines and dashed lines, respectively: (a) the first excited state S_1 simulation, (b) the second excited state S_2 simulation, (c) the third excited state S_3 simulation. Red solid and dashed curves correspond, respectively, to the original LUMO (now occupied) and to the original HOMO (now unoccupied).
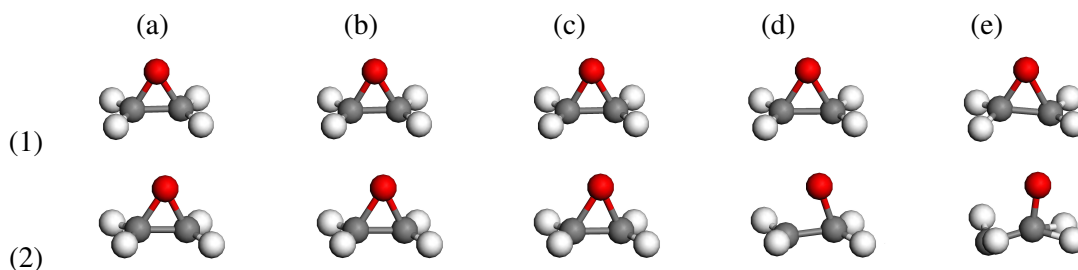
Figure 4.12: Snapshots of the photochemical ring opening of oxirane molecule at the first and second excited state simulation using TDGW: (1) The S_1 simulation (a) 20 fs, (b) 40 fs, (c) 50 fs, (d) 70fs, and (e) 80 fs. (2)The S_2 simulation (a) 20 fs, (b) 30 fs, (c) 40 fs, (d) 50fs, and (e) 60 fs.
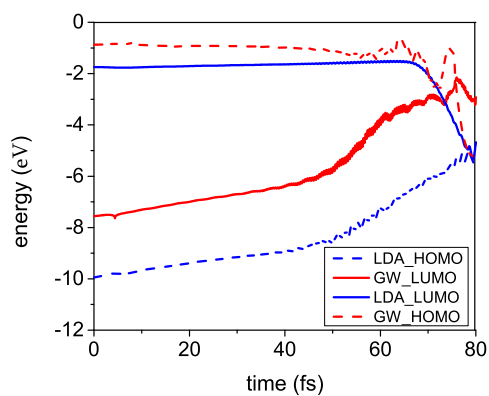

Figure 4.13: The Kohn-Sham eigenenergies (blue lines) and the quasiparticle energies (red lines) of HOMO (unoccuppied) and LUMO (occuppied) level for the first excited state S_1 simulation.

Chapter 5

Conclusion

In this thesis, several interesting chemical reactions were investigated by performing the ab initio molecular dynamics (AIMD) based on the time-dependent density functional theory (TDDFT) and time-dependent GW (TDGW) methods. The AIMD simulation helps to study not only the reaction pathways but also the time evolution of electronic states. In Chapter 3, one of the possible reaction pathway of the hydrogenation of carbon monoxide producing methanol was presented. Methanol is an useful energy carrier, easy to store in compare with hydrogen and burns cleaner than fossil fuel. It plays a very important role in chemical industry and it can be use as a fuel for specialised vehicles [54]. Methanol can be produced from the hydrogenation of CO. Carbon monoxide (CO) is one of the important basic molecules to produce organic compounds. Hydrogen atoms might react step by step with carbon monoxide as: $H + CO \rightarrow HCO$ (a), $H + HCO \rightarrow H_2CO$ (b) and then $2H + H_2CO \rightarrow CH_3OH$ (c). The reaction (a) has to be carried out through the excited state, which one electron was excited from the highest occupied molecular orbital (HOMO) level to the lowest unoccupied molecular orbital (LUMO) level. We succeeded in reproducing this reaction at the excited state by using the TDGW method. The reaction (b) and the reaction (c) can proceed through the ground state within the chosen initial condition.

In Chapter 4, the photochemical ring opening reaction of oxirane molecule was studied by the AIMD in the first three excited states. Oxirane (C_2H_4O) is the simplest epoxide with a three-membered ring consisting of one oxygen atom and two carbon atoms. The ring-opening reaction of oxirane is very important to study other electrocyclic reaction, for example ring-opening reaction of vitamin D. It is believed that this

reaction happens around the crossing region between the energy levels [71]. Oxirane is a small molecule where the photochemistry is expected to be handled with the non-adiabatic TDDFT/TDGW molecular dynamics simulation and provides a simple prototype for investigation of more complicated photochemical reactions [71]. The rapid CO ring opening of oxirane molecule was discovered during the second excited state simulation. This reaction proceeded more difficulty in the first and third excited state. These results are in a good agreement with those of other groups [72, 73]. Our TDLDA/TDGW non-adiabatic quantum molecular dynamics (NAQMD) simulation seems working good, because the change of geometry follows immediately at the point of level crossing between two levels of quasiparticle energy. The optical absorption spectra of oxirane was also calculated by using the $GW+$ Bethe-Salpeter equation (BSE) method. The results showed the contribution of some of the main electronic transition between energy levels to the first, second and third absorbed states of the spectra.

In these studies, the TDGW method was introduced in the all-electron mixed basis code, TOMBO, to perform the electronic excited state dynamics simulations. To the best of our knowledge, we are the first group in the world doing the ab initio molecular dynamics based on the GW method. The excited state dynamics, which were performed within the TDGW approach, gave the good results in comparison with the TDDFT dynamics simulation within the A-LDA.

Almost all photochemical ring-opening reactions investigated in this study occur in the region of crossing between the energy levels. In this region, the non-adiabatic transition will occur and the adiabatic approximation breaks down. I implemented the NAQMD routine in the TOMBO code to treat the non-adiabatic process in the dynamics simulation. The photochemical ring-opening reaction of oxirane molecule were performed by using the TDDFT and TDGW methods including the new NAQMD implementation.

Overall, the simulations were performed with zero initial velocities except for the ground state simulation of the H + CO reaction. Generally, if one wants to simulate a reaction at a certain temperature, all atoms need to be assigned velocities in the initial state. However, in the case of H + HCO and 2H + H_2CO, it may be not necessary to introduce the initial velocities, because the reactions clearly proceeded without initial velocities. For the case of oxirane, the simulation at finite temperature will be left for the future study.

NAQMD could be called as time-dependent density functional theory based on the Ehrenfest dynamics [92]. As well known in Ehrenfest dynamics, electrons follow the time-dependent Schrödinger equation and the nuclei move on an averaged potential surface that involves several electronic states. This method consists of the purely classical treatment of nuclei, so the extended formalism which includes quantum effects in the nuclear dynamics need to be considered in the future.

Appendix A

Calculation of non-adiabatic coupling

In the all electron mixed basis approach, as in Eq. (2.56) The Kohn–Sham wavefunction is expanded in terms of PWs and AOs as follows

$$\phi_\nu(\mathbf{r}) = \frac{1}{\sqrt{\Omega}} \sum_{\mathbf{G}} c_\nu^{PW}(\mathbf{G}) e^{i\mathbf{G}\cdot\mathbf{r}} + \sum_j \sum_{nlm} c_\nu^{AO}(jnlm) \phi_{jnlm}^{AO}(\mathbf{r} - \mathbf{R}_j) \equiv \sum_\xi c_{\nu,\xi} f_\xi(\mathbf{r}) \tag{A.1}$$

The non-adiabatic coupling vector:

$$d_{\alpha\beta}^I = \langle \phi_\alpha | \nabla_I | \phi_\beta \rangle \tag{A.2}$$

can be calculated as follow:

$$d_{\alpha\beta}^I = \langle \mathbf{G}_\alpha | \nabla_{\mathbf{I}} | \phi_\beta^{AO} \rangle + \langle \phi_\alpha^{AO} | \nabla_{\mathbf{I}} | \mathbf{G}_\beta \rangle + \langle \mathbf{G}_\alpha | \nabla_{\mathbf{I}} | \mathbf{G}_\beta \rangle + \langle \phi_\alpha^{AO} | \nabla_{\mathbf{I}} | \phi_\beta^{AO} \rangle \tag{A.3}$$

Because the planewave fucntions do not depend explicitly on $\mathbf{R}_I$ so the second term and the third term of Eq. (A.3) are 0. We will have:

$$d_{\alpha\beta}^I = \langle \mathbf{G}_\alpha | \nabla_{\mathbf{I}} | \phi_\beta^{AO} \rangle + \langle \phi_\alpha^{AO} | \nabla_{\mathbf{I}} | \phi_\beta^{AO} \rangle \tag{A.4}$$

For the fist term:

$$\langle \mathbf{G}_\alpha | \nabla_\mathbf{I} | \phi_\beta^{AO} \rangle = \frac{1}{\sqrt{\Omega}} \int e^{-i\mathbf{G}_\alpha \mathbf{r}} \nabla_I \phi_\beta^{AO}(\mathbf{r} - \mathbf{R}) dr$$

$$= \frac{1}{\sqrt{\Omega}} \nabla_I \int e^{-i\mathbf{G}_\alpha \mathbf{r}} \phi_\beta^{AO}(\mathbf{r} - \mathbf{R}) dr$$

$$= \frac{1}{\sqrt{\Omega}} \nabla_I \int e^{-i\mathbf{G}_\alpha(\mathbf{r}' + \mathbf{R})} \phi_\beta^{AO}(\mathbf{r}') dr$$

$$= \frac{1}{\sqrt{\Omega}} \nabla_I e^{-i\mathbf{G}_\alpha \mathbf{R}} \int e^{-i\mathbf{G}_\alpha \mathbf{r}'} \phi_\beta^{AO}(\mathbf{r}') dr$$

$$= -\frac{i\mathbf{G}_\alpha}{\sqrt{\Omega}} e^{-i\mathbf{G}_\alpha \mathbf{R}} \int e^{-i\mathbf{G}_\alpha \mathbf{r}'} \phi_\beta^{AO}(\mathbf{r}') dr \tag{A.5}$$

Using:

$$\int e^{-i\mathbf{G}_\alpha \mathbf{r}'} \phi_\beta^{AO}(\mathbf{r}') dr = \langle G_\alpha | \phi_\beta^{AO} \rangle \tag{A.6}$$

we get:

$$\langle \mathbf{G}_\alpha | \nabla_\mathbf{I} | \phi_\beta^{AO} \rangle = (-i\mathbf{G}_\alpha) \langle G_\alpha | \phi_\beta^{AO} \rangle \tag{A.7}$$

Calculation of quasiparticle energies

The quasiparticle energies ϵ_n^{QP} and wave function $\phi_n(\mathbf{r})$ can be obtained by solving the following coupled equation:

$$(T + V_{Hatree} + V_{ext})\phi_n(\mathbf{r}) + \int d\mathbf{r}' \Sigma_{xc}(\mathbf{r}, \mathbf{r}'; \epsilon_n^{QP})\phi_n(\mathbf{r}) = \epsilon_n^{QP}\phi_n(\mathbf{r}), \tag{B.1}$$

$$\Sigma_{xc}(\mathbf{r}, \mathbf{r}'; \epsilon_n^{QP}) = \frac{i}{2\pi} \int d\omega' G(\mathbf{r}, \mathbf{r}'; \omega + \omega')W(\mathbf{r}, \mathbf{r}'; \omega')e^{i\eta\omega'}, \tag{B.2}$$

here T, V_{Hatree} and V_{ext} are the kinetic energy operator, the external potential, and the Hatree potential, respectively. Σ_{xc} denotes the electron self-energy containing the effect of exchange-correlation between electrons. η is a positive infinitesimal number. $W = \epsilon^{-1}U$ is the dynamically screened Coulomb interaction in the random-phase approximation (RPA), here U is the bare Coulomb interaction. ϵ denotes the dielectric function

$$\epsilon = 1 - UP \tag{B.3}$$

where $P = -iGG$ is the polarizability. In this approach, the generalized plasmon pole (GPP) model [14] is used to evaluate the self-energy. The one-particle Green's function G is written in the form

$$G(\mathbf{r}, \mathbf{r}'; \omega') = \sum_{n'} \frac{\phi_{n'}(\mathbf{r})\phi_{n'}^*(\mathbf{r}')}{\omega - \epsilon_{n'} - i\delta_{n'}}, \tag{B.4}$$

where $\delta_{n'} = 0^+$ for $\epsilon_{n'} < \mu_F$ and $\delta_{n'} = 0^-$ for $\epsilon_{n'} > \mu_F$ (μ_F is the Fermi energy). In general, $\phi_{n'}(\mathbf{r})$ and $\epsilon_{n'}^{QP}$ are replaced by the LDA wave functions and eigenvalues, respectively. Finally, one can obtain the

quasiparticle energies in terms of first-order perturbation theory by the following equation:

$$\epsilon_n^{QP} \simeq \epsilon_n^{LDA} + \int d\mathbf{r} \int d\mathbf{r}' \phi_n^*(\mathbf{r}) \Big[\Sigma_{xc}(\mathbf{r}, \mathbf{r}', \epsilon_n^{QP}) - V_{xc}^{LDA}(\mathbf{r}) \delta(\mathbf{r} - \mathbf{r}') \Big] \phi(\mathbf{r}'), \qquad (B.5)$$

where ϵ_n^{LDA} denotes the corresponding LDA eigenvalues.

Bibliography

[1] D. Frenkel and B. Smit, *Understanding Molecular simulation. From Algorithms to Applications*, (Academic Press, Boston, 1996).

[2] D. Marx, J. Hutter, *Ab Initio Molecular Dynamics Basic Theory and Advanced Methods*, (Cambridge University Press, Cambridge, 2009).

[3] M. C. Payne, M. P. Teter, D. C. Allan, T. A. Arias, and J. D. Joannopoulos. Reviews of Modern Physics, **64**, 1045 (1992).

[4] D. K. Remler and P. A. Madden, Molecular Physics, **70**, 921, (1990).

[5] V. Bonacic-Koutecky and R. Mitric, Chem. Rev. **105**(1), 11 (2005).

[6] M. D. Hack and D. G. Truhlar, J. Phys. Chem. **A 104**, 7917 (2000).

[7] M. Born and K. Huang. Dynamical theory of crystal lattices. Clarendon Press, OXford, Nov. 1954. ISBN 9780198503699.

[8] M. Born and R. Oppenheimer. Zur Quantentheorie der Molekeln. *An − nalenderPhysik*, 84:457484, (1927).

[9] J. C. Williamson, J. Cao, H. Ihee, H. Ihee, H. Frey and A. H. Zewail, Nature **386**, 159 (1997).

[10] S. A. Harich, D. Dai, C. C. Wang, X. Yang, S. D. Chao and R. T. Skodje, Nature **419**, 281 (2002).

[11] E. Runge and E. K. U. Gross, Phys.Rev **52**, 997 (1984).

[12] K. Ohno, K. Esfarjani, and Y. Kawazoe, *Computational Materials Science: From Ab Initio to Monte Carlo Methods*, Springer Series in Solid State Sciences, Vol.129 (Springer Verlag, Berlin and Heidelberg, 1999).

[13] L. Hedin, Phys. Rev. **139**, A796 (1965).

[14] M. S. Hybertsen and S. G. Louie, Phys. Rev. B **34**, 5390 (1986).

[15] R. W. Godby, M. Schlüter, and L. J. Sham, Phys. Rev. B **37**, 10159 (1988).

[16] K. Morokuma and S. Iwata, Chem. Phys. Lett. **16**, 192 (1972).

[17] U. Saalmann and R. Schmidt, Z. Phys. **D38**, 153, (1996).

[18] S. Ono, Y. Noguchi, R. Sahara, Y. Kawazoe, and K. Ohno, Computer Phys. Comm. **189**, 20 (2015).

[19] K. Ohno, F.Mauri, and S.G .Louice, Phys. Rev. B **56**, 1009, (1997).

[20] T. Ohtsuki, K. Ohno, K. Shiga, Y. Kawazoe, Y. Maruyama and K. Masumoto, Phys. Rev. Lett. **81**, 967 (1998).

[21] T. Ohtsuki, K. Ohno, K. Shiga, Y. Kawazoe, Y. Maruyama and K. Masumoto, Phys. Rev. Lett. **B60**, 1531 (1999).

[22] Y. Kodama, S. Ishi and K. Ohno, J. Phys. Cond.Matter **19**, 365242 (2007).

[23] Y. Kodama and K. Ohno, Appl. Phys. Lett. **96**, 034101 (2010).

[24] T. N. Pham, S. Ono and K. Ohno, J. Chem. Phys., **144**, 144309 (2016).

[25] N. L. Doltsinis, *Nonadiabatic Dynamics: Mean-Field and Surface Hopping*, in J. Grotendorst, D. Marx and A. Muramatsu, editors, *Quantum Simulations of Complex Many-body Systems: From Theory to Algorithms, Lecture Notes*, **10**, 377, John von Neumann Institute for Computing, NIC Series (2002).

[26] J. C. Tully, J. Chem. Phys. **93 (2)**, 1061 (1990).

[27] D. Marx and J. Hutter. *Modern Methods and Algorithms of Quantum Chemistry*, NIC Series **1**, 301 (2000).

[28] W. Domcke, D. R. Yarkony, and H. Kppel, editors. *Conical Intersections: Electronic Structure, Dynamics & Spectroscopy*, Advanced Series in Physical Chemistry, **15** (2004).

[29] R. M. Dreizler and E. K. U. Gross. *Density Functional Theory*, Springer, Berlin, (1990).

[30] F. Nogueira, A. Castro, and M. A. L. Marques, editors. *A Primer in Density Functional Theory*, volume 620 of Lect. Notes. Phys. (2003).

[31] E. Tapavicza, *Development of a Non-Adiabatic Ab Initio Molecular Dynamics Method and its Application to Photodynamical Processes*, PhD thesis, École polytechnique fédérale de Lausanne, France, (2008).

[32] P. Hohenberg and W. Kohn. Phys. Rev., **136**, B864, (1964).

[33] W. Kohn and L. Sham. Phys. Rev., **140(4A)**, A1133 (1965).

[34] R. V. Leeuwen, Phys. Rev. Lett, **80**, 6, (1280).

[35] R. Schmidt, O. Knospe and U. Saalmann Il Nuovo. Chim., **A110**, 1201, (1997).

[36] U. Saalmann and R. Schmidt, Phys. Rev. Lett., **80**, 3213, (1998).

[37] O. Knospe, U. Saalmann, J. Jellinek and R. Schmidt, Eur. Phys. J, **D5**, 1, (1999) .

[38] T. Kunert and R. Schmidt, Phys. Rev. Lett., **86**, 5258, (2001).

[39] S.G.Louie, K.-M.Ho and M.L.Cohen, Phys. Rev. B **19**, 1774 (1979).

[40] T. Sawada, J. Wu, Y. Kawazoe, and K. Ohno, Trans. Mater. Res. Soc. Jpn. **29**, 3727 (2004).

[41] T. Sawada, Y. Kawazoe, and K. Ohno, Sci. Tech. Adv. Mater. **5**, 689 (2004).

[42] T. Sawada and K. Ohno, Chem. Phys. Lett. **405**, 234 (2005).

[43] S. E. Koonin, *Computational Physics*, (Addison-Wesley, New York, 1986).

[44] A. Goldberg, H.M. Schey, J.L. Schwartz, Am. J. Phys. **35**, 177 (1967).

[45] J. J. Sakurai, *Modern Quantum Mechanics*, (Benjamin/Cummings Publishing, Menlo Park, 1985).

[46] Y. Kodama, *Excited-state dyanmics simulations of a π-conjugated dendrimer and molecular hetero-junction of C_{60} towards organic thin film solar cells*, PhD thesis, Yokohama National University, Japan (2010).

[47] K. M. Ho, C. Elsasser, C. T. Chan, and M. Fahnle, J. Phys. Condens. Matter **4**, 5189 (1992).

[48] P. Bhattacharya, R. Fornari, H. Kamimura, *Comprehensive semiconductor science and technology*, **1**(Van Nostrand Reinhold Company, New York, 1979).

[49] L. C. Grabow and M. Mavrikakis, ACS Catal. **1**, 365 (2011).

[50] M. Arsalanfar, A. A. Mirzaei, H. R. Bozorgzadeh and A. Samimi Phys. Chem. Res. **2** (2), 179 (2014).

[51] R. D. Rempt, Phys. Rev. Lett. **22**, 1034 (1969).

[52] R. Sahara, H. Mizuseki, M. H. F. Sluiter, K. Ohno, and Y. Kawazoe, RSC Advances, **3**, 12307 (2013).

[53] F. Studt, A. Pedersen, Q. Wu, A. D. Jensen, B. Temel, J. D. Grunwaldt, J. K. Norskov, Journal of Catalysis, **293**, 51, (2012).

[54] W. H. Cheng, H. H. Kung /it Methanol Production and Use, CRC PRess,

[55] S.Wang, E. E. Dames, D. F. Davidson and R. K. Hanson, J. Phys. Chem. A **118**, 10201 (2014).

[56] J. A. Miller, R. J. Kee, and C.K. Westbrook, Annual. Rev. Phys. Chem. **41**, 345 (1990).

[57] M. Keceli, T. Shiozaki, K. Yagi, and S. Hirata, Mol. Phys. **107**, 1283 (2009).

[58] P. S. Peters, D. Duflot, L. Wiesenfeld, and C. Toubin, J. Chem. Phys. **139**, 164310 (2013).

[59] K. Tanaka and E. R. Davidson, J. Chem. Phys. **70**, 2904 (1979).

[60] L. Song, A. V. D. Avoird, and G. C. Groenenboom, J. Phys. Chem. A **117**, 7571, (2013).

[61] Jr. T. H. Dunning, J. Chem. Phys. **73**, 2304 (1980).

[62] H. Romanowski, K. T. Lee, J. M. Bowman and L. B. Harding, J. Chem. Phys. **84**, 4888 (1986).

[63] M. Bittererová, H. Lischka, S. Biskupič, Int. J. Quantum Chem. **55**, 261 (1955).

[64] J. Franck and E. G. Dymond, Trans. Faraday Soc. **21**, 536, (1926).

[65] K. P. Huber and G. Herzberg, *Molecular Spectra and Molecular Structure: IV. Constants of Diatomic Molecules*, (Elsevier B. V., 2011).

[66] J. M. Dyke, J. Chem. Soc. Faraday Trans. **83**, 69 (1987).

[67] K. K. Murray, T. M. Miller, D. G. Leopold, and W. C. Lineberger, J. Chem. Phys. **84**, 2520 (1986).

[68] J. M. Brown and D. A. Ramsay, Can. J. Phys, **53**, 2232 (1975).

[69] L.V. Gurvich; I. V. Veyts and C. B. Alcock, *Thermodynamic Properties of Individual Substances*, (Fouth Edition, Hemisphere Pub. Co., New York, 1989).

[70] P. Venkateswarlu, W. Gordy, J. Chem. Phys. **23** (7), 1200 (1955).

[71] F. Cordova, L. J. Doriol, A. Ipatov, and M. E. Casida, J. Chem. Phys. **127**, 164111, (2007).

[72] E. Tapavicza, I. Tavernelli, U. Rothlisberger, C. Filippi, and M. E. Casida, J. Chem. Phys. **129**, 124108 (2008).

[73] Jian-Hao Li, T. J. Zuehlsdorff, M. C. Payne and N. D. M. Hine, Phys. Chem. Chem. Phys. **17**, 12065 (2015).

[74] M.Rohlfing and S. G. Louie, Phys. Rev. B **62**, 4927 (2000).

[75] G. Onida, L. Reining, and A. Rubio, Rev. Mod. Phys. **74**, 601 (2002).

[76] M. L. del Puerto, M. L. Tiago, and J. R. Chelikowsky, Phys. Rev. Lett. **97**, 096401 (2006).

[77] M. L. del Puerto, M. L. Tiago, and J. R. Chelikowsky, Phys. Rev. B **77**, 045404 (2008).

[78] Y. Noguchi and K. Ohno, Phys. Reb. A **81**, 045201 2010.

[79] R. Kuwahara, Y. Noguchi, K. Ohno, Phys. Rev. B **94**, 121116 (R) (2016).

[80] Y. Noguchi, S. Ishii, K. Ohno, and T. Sasaki, J. Chem. Phys. **129**, 104104 (2008).

[81] K. Ohno, M. Tanaka, J. Takeda and Y. Kawazoe, *Nano-and Micromaterials*, Series on Advances in Materials Research, Vol.9 (Springer-Verlag, Berlin, 2008) and the references therein.

[82] Y. Ma, M. Rohfling, and C. Molteni, Phys. Rev. B **80**, 241405(R) (2009).

[83] K. Ohno, Sci. Tech. Adv. Mat. **5**, 603 (2004).

[84] G. Strinati, Phys. Rev. B **29**, 5718 (1984).

[85] K. Ohno, F. Mauri, and S. G. Louie, Phys. Rev. B **56**, 1009 (1997).

[86] S. Ishii, K. Ohno, Y. Kawazoe, and S. G. Louie, Phys. Rev. B **65**, 245109 (2002).

[87] Y. Noguchi, S. Ishii, and K. Ohno, J. Chem. Phys. **125**, 114108 (2006).

[88] M. Kawasaki, T. Ibuki, M. Iwasaki, and Y. Takezaki, J. Chem. Phys. **59**, 2076 (1973).

[89] C. Hirose, Bull. Chem. Soc. Jpn. **47**, 1311 (1974).

[90] NIST Chemistry Webbook (http://webbook.nist.gov/chemistry).

[91] E. Gomer and J. W. A. Noyes, J. Am. Chem. Soc. **72**, 101 (1950).

[92] M. Fischer, J. Handt, and R. Schmidt, Phys. Rev. A **90**, 012525 (2014).

Acknowledgments